Carbohydrate Polymer Technologies and Applications 8 (2024) 100587

Contents lists available at ScienceDirect

Carbohydrate Polymer Technologies and Applications

journal homepage: www.sciencedirect.com/journal/carbohydrate-polymer-technologies-and-applications

Creation of 3D chitin/chitosan composite scaffold from naturally pre-structured verongiid sponge skeleton

Izabela Dziedzic [a,b,*], Kamil Dydek [b,c,*], Jakub Trzciński [d,e], Anna Boczkowska [c], Alona Voronkina [f], Teofil Jesionowski [g], Hermann Ehrlich [b,g,*]

[a] Faculty of Chemistry, Adam Mickiewicz University, 8 Uniwersytetu Poznańskiego St., 61-614 Poznan, Poland
[b] Centre of Advanced Technologies, Adam Mickiewicz University in Poznan, 10 Uniwersytetu Poznanskiego St., 61-614 Poznan, Poland
[c] Faculty of Materials Science and Engineering, Warsaw University of Technology, 141 Woloska St., 02-507 Warsaw, Poland
[d] Centre for Advanced Materials and Technologies CEZAMAT, Warsaw University of Technology, Poleczki 19, 02-822 Warsaw, Poland
[e] Department of Biotechnology and Bioprocess Engineering, Faculty of Chemical and Process Engineering, Warsaw University of Technology, Warynskiego 1, 00-645 Warsaw, Poland
[f] Pharmacy Department, National Pirogov Memorial Medical University, Vinnytsya, Pirogov str. 56, 21018 Vinnytsia, Ukraine
[g] Faculty of Chemical Technology, Institute of Chemical Technology and Engineering, Poznan University of Technology, Berdychowo 4, 60-965 Poznan, Poland

ARTICLE INFO

Keywords:
Chitin
Chitosan
Scaffolds
Composite
Marine sponges
Zeta potential

ABSTRACT

This study represents the first creation and characterization of a 3D chitin/chitosan composite scaffold derived from the naturally pre-structured skeleton of the cultivated marine demosponge *Aplysina aerophoba*, aiming to preserve the intricate architecture of the unique tube-like chitin while incorporating chitosan layers. Advanced staining methods, including the use of iodine and Cibacron Brilliant Red (CBR), were employed to distinguish these polysaccharides. ATR-FTIR spectroscopy confirmed the system's structural integrity and identified the optimal chitin/chitosan balance, achieved after 60-minute treatment in 38 % NaOH at 95 °C. Fluorescent microscopy using fluorescein isothiocyanate (FITC) effectively confirmed the presence of chitosan layers in the created chitin/chitosan scaffolds. Scanning electron microscopy analysis further elucidated significant morphological distinctions, where chitin fibers displayed a smooth, uniform surface, contrasting with the ragged and irregular texture of chitosan-containing fibers, indicating significant surface modifications. Zeta potential measurements confirmed the partial transformation of chitin into chitosan. The dual-layer configuration, consisting of a resilient chitin core and a versatile chitosan exterior, not only provides structural support, but also enhances the scaffold's functionality for potential technological and biomedical applications. The preferential metallization of the chitosan phase by copper nanoparticles in the created 3D chitin/chitosan composite opens the way to the potential use of such scaffolds in catalysis.

1. Introduction

In addressing current needs relating to modern technologies in the field of structural biomimetics, significant emphasis is placed on sophisticated three-dimensional (3D) manufacturing processes (Prem Ananth & Jayram, 2024). Diverse fabrication techniques and special manufacturing methods have recently been reviewed in the literature (Abdelaziz et al., 2023; Suamte et al., 2023). Both synthetic and naturally occurring materials (i.e. biomaterials) (Nikolova & Chavali, 2019) are crucial for the development of corresponding scaffolds for effective application in technology and biomedicine (Li et al., 2020; Shimojo et al., 2020). Essential to tissue engineering, 3D scaffolds are required to meet strict guidelines, including delivering precise structural and mechanical prompts for use in technological applications and ensuring bio- and eco-compatibility, along with particular biological, immunological, and physicochemical properties qualifying them for use in this field (Tsurkan et al., 2021). The pivotal criterion for such scaffolds is their ability to support optimal cell growth, differentiation, and proliferation (Wysokowski et al., 2023), thereby unlocking their potential applications across diverse fields of modern biomedicine. In modern scaffolding strategies (Tsurkan et al., 2021) two clear directions have emerged: the optimization of methods for producing synthetic scaffolds to ensure their structural and functional similarity to corresponding biological structures (Flores-Jiménez et al., 2023), and the use of pre-structured

* Corresponding authors.
E-mail addresses: izabela.dziedzic@amu.edu.pl (I. Dziedzic), kamil.dydek@pw.edu.pl (K. Dydek), herehr@amu.edu.pl (H. Ehrlich).

https://doi.org/10.1016/j.carpta.2024.100587

Available online 10 October 2024

biomaterials that already exist in nature in the form of skeletons – conditional, of course, on the renewability of such biological raw materials (Khrunyk et al., 2020; Krishani et al., 2023; Unnithan et al., 2018).

In the pursuit of biomimetic approaches, recent biomaterials-inspired research has focused on naturally pre-fabricated skeletal structures of marine origin, particularly those with the unique 3D architecture found in skeletons of diverse sponges (Porifera) (Ehrlich, Luczak, et al., 2022; Ehrlich et al., 2024; Jesionowski et al., 2018; Voronkina et al., 2023). In particular, the exoskeletons of marine sponges of the class Demospongiae, optimized over more than 800 million years of evolution (Ehrlich et al., 2013), represent unique, mechanically stable, fiber-based, micro-, and macroporous biocomposite 3D constructs made of collagen-like spongin (Petrenko et al., 2019) or aminopolysaccharide chitin (Klinger et al., 2019), with or without inclusions of diverse mineral phases. Under marine farming conditions, both keratosan and verongiid demosponges, with spongin- and chitin-based skeletons respectively, are recognized as organisms of value to the marine bioeconomy, with high skeleton regeneration rates (Bierwirth et al., 2022; Binnewerg et al., 2020) and consequently offering high large-scale potential (Tsurkan et al., 2021; Amato et al., 2024).

Chitin, an abundant structural biopolymer characterized by β-1,4-linked N-acetylglucosamine units, manifests in three polymorphs: alpha-, beta-, and gamma-chitin (Kaya et al., 2017, 2018). The chemistry, analytics and material properties of chitin are well studied (for overview see Joseph et al., 2021; Kadokawa, 2024; Kertmen & Ehrlich, 2022; D. Tsurkan et al., 2021; M.V. Tsurkan et al., 2021). Alpha-chitin alone has been documented in nearly twenty marine and three freshwater sponge species (Talevski et al., 2020). Of particular note is the distinctive 3D microfibrous and macroporous architecture exhibited by poriferan chitin, especially in species of the order Verongiida (class Demospongiae). In diverse representatives of this order, naturally pre-fabricated tubular scaffolds, both 3D cylindrical (Nowacki et al., 2022) and flat (Kertmen et al., 2021), characterize their skeletal morphology (Ehrlich et al., 2010). These distinctive attributes imply excellent prospects for the successful utilization of such ready-to-use scaffolds across diverse applications, including uranium waste treatment (Schleuter et al., 2013), tissue engineering (Choi & Ben-Nissan, 2019; Mutsenko et al., 2019), and the advanced field within materials science known as extreme biomimetics (Ehrlich et al., 2022; Wysokowski et al., 2015). The tube-like chitin of verongiids has also been studied with regard to its capillarity, with possible applications in drug release (Kovalchuk et al., 2019; Schubert et al., 2019). In addition, the material properties of chitinous matrices of sponge origin have recently been studied (for details see Duminis et al., 2023; Dziedzic et al., 2023).

To our best knowledge, there are no reports on the use of poriferan chitin scaffolds for the production of chitosan. This is logical, because there is no need to destroy poriferan chitin, uniquely pre-structured in the form of scaffolds, to obtain powdered chitosan, as happens when raw materials from fungi or crustaceans are used (Kou et al., 2021; Kozma et al., 2022). Chitosan, a derivative of chitin obtained commonly from the microfibrils of crustacean shells, is a biopolymer known for its extensive application in diverse fields due to its biocompatibility and biodegradability (for overview see Kertmen et al., 2023). Chitosan constitutes a family of polymers comprising extended chains of N-acetylglucosamine units. It is categorized based on its degree of deacetylation, which may be low (55–70 %), medium (70–85 %), high (85–95 %) or ultrahigh (95–100 %) (Lv, 2016). Within a molecular weight range of 50–2000 kDa, chitosan exhibits insolubility in water and alkaline solutions, yet it readily dissolves in nearly all aqueous acids. Its biological activity is intricately linked to the positioning of sulfate groups within glucosamine residues (Nuc & Dobrzycka-Krahel, 2021). The presence of polar groups imparts excellent hygroscopicity, moisture retention (Xing et al., 2018), and electrostatic attraction, thereby facilitating mucoadhesion (Sogias et al., 2008).

Chitosan production currently relies on both biological and chemical approaches (Kertmen et al., 2023). The biological strategy leverages chitin deacetylase, providing a pathway that is notably more sustainable and less environmentally harmful. Nevertheless, the higher costs and fluctuating degrees of deacetylation (DD%) associated with this method place constraints on its attractiveness for industrial applications (Younes & Rinaudo, 2015). Chemically, chitosan is produced by treating chitin with a strong alkaline solution, often at above 100 °C, over extended periods, with NaOH concentrations reaching up to 50 % and in some instances even 70 % (Sivashankari & Prabaharan, 2017). The degree of deacetylation increases with the duration of the reaction, temperature, and the concentration of the base, and although this method results in a reduction of molecular weight and generates significant amounts of toxic wastewater, its simplicity and effectiveness mean that it remains the preferred industrial process (Gîjiu et al., 2022). Furthermore, recent investigations have considered the application of ionic liquids for the deacetylation of chitin, uncovering their potential to augment the activity of chitin deacetylase and elevate the degree of deacetylation in chitosan (Ma et al., 2020). Notwithstanding these benefits, the high costs, prolonged reaction times, and ecological implications associated with the use of ionic liquids pose significant barriers to their broad integration within industrial practices. Chitosan has been used for the manufacture of various types of membranes, porous films and scaffolds (Beleño Acosta et al., 2023; Gholap et al., 2024; Jana et al., 2012). All such processes entail the use of additional reagents and energy costs (Bergonzi et al., 2019; Królczyk et al., 2020; Tyliszczak et al., 2020), because the chitosan powder must be transformed into 3D constructs.

However, in the case of pre-existing poriferan chitin 3D scaffolds, these problems are no longer present. The motivating goal of the present study was to confirm the possibility of obtaining chitosan layers on the surface of mechanically robust sponge chitin fibers in such a way that the unique architecture of the 3D chitin skeleton remains exceptionally preserved. The aim of the work, then, was to create a structural chitin/chitosan composite matrix resembling the size and shape of an initial chitin-based sponge skeleton, here using the example of the cultivated marine demosponge *Aplysina aerophoba*. While chitin/chitosan composites have been reported in some previous studies (Anandhavelu et al., 2017; Mushi et al., 2014; Sivanesan et al., 2021), the distinctive and innovative feature of the present work is the assembly of 3D scaffolds that make use of these biopolymers' inherent advantages. The potential scalability of the manufacturing process, coupled with the scaffolds' adaptability to various biomedical uses, underscores the significance of this advance. By exploring the frontier of chitin/chitosan-based 3D scaffolding, this work aims to provide a foundation for future innovations in regenerative medicine and tissue engineering, heralding a new era of development of bio-compatible and sustainable biomaterials of marine origin.

2. Materials and methods

2.1. Isolation of chitin scaffolds from Aplysina aerophoba

Sponges identified as *Aplysina aerophoba* (Nardo, 1833) by Prof. Zoran Klijaic (Institute of Marine Biology, Montenegro) in 2008 (Fig. 1 a) were carefully gathered using scuba diving methods from Kotor Bay, Montenegro, part of the Adriatic Sea, at depths ranging from 3 to 5 m, in close proximity to a marine aquaculture facility.

In the first stage of processing, the sponges were submerged in 500 ml of distilled water and subjected to ultrasonic treatment for a duration of 1 h at ambient temperature. They were next immersed in approximately 500 ml of a 20 % acetic acid solution (STANLAB Sp. z o.o., Lublin, Poland), and subjected to a 2 h sonication process in an ultrasonic bath (Bandelin, Berlin, Germany) with the temperature maintained at 40 °C. Following this step, the acetic acid solution was replaced with a fresh batch, and the samples were subjected to an additional 2 h of sonication. The obtained sponge skeletons were subsequently rinsed

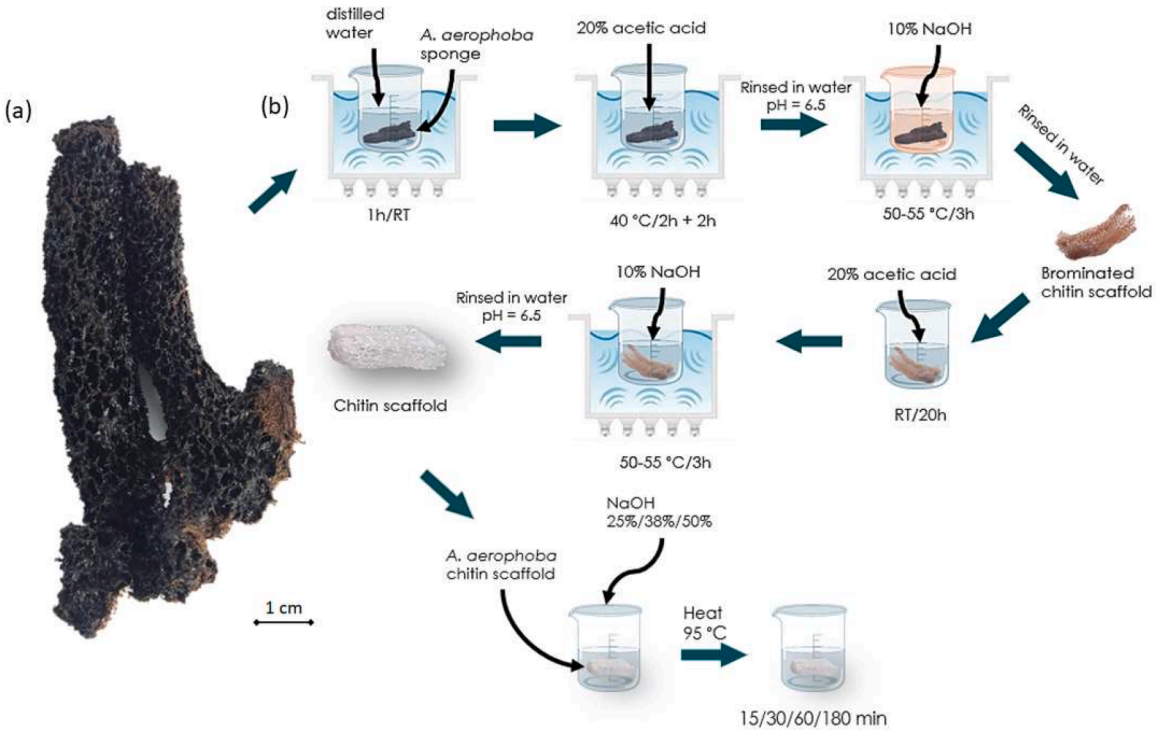

Fig. 1. (a) Selected sample of dried *Aplysina aerophoba* sponge used in the study; (b) schematic representation of the process of isolating chitin scaffolds and preparing 3D chitin/chitosan scaffolds from *A. aerophoba* demosponge.

with distilled water until reaching a pH of 6.5, and were then immersed in 500 ml of a 10 % NaOH solution (Sigma Aldrich, St. Louis, MO, USA) and subjected to sonication for 3 h with the temperature maintained within a range of 50–55 °C. The resulting skeleton scaffolds (see Fig. 1 b) were rinsed with water and immersed in a 20 % acetic acid solution for approximately 20 h to eliminate any residual calcium carbonate debris. Following this, the scaffolds were submerged in a fresh 200 ml solution of 10 % NaOH and subjected to a 3-hour sonication process at 50–55 °C. Finally, the resulting colorless chitin scaffolds were thoroughly washed with distilled water until a pH of 6.5 was reached.

2.2. Preparation of 3D chitin/chitosan scaffolds

The process of deacetylation applied to the sponge chitin samples involved treatment at a temperature of 95 °C, employing NaOH solutions sourced from Sigma Aldrich (St. Louis, MO, USA) with concentrations of 25 %, 38 %, and 50 % (Fig. 1 b). These treatments were administered for different durations, namely 15, 30, 60, and 180 min, to determine the differential effects. The primary objective of this research was to fabricate a 3D composite structure that would combine chitin's structural skeleton with chitosan's versatile properties and its potential for further chemical modifications due to its solubility in acidic aqueous solutions (Harugade et al., 2023). To achieve this, chitin sourced from *A. aerophoba* sponge skeleton underwent deacetylation at 95 °C at selected time intervals in NaOH solutions of 25 %, 38 %, and 50 % concentrations to form a chitin/chitosan scaffold. However, it was observed that samples treated with 50 % NaOH exhibited instability, losing their three-dimensional integrity during neutralization, while those treated with 25 % NaOH underwent discoloration in an iodine test. For these reasons, further work was focused on the analysis of 3D chitin/chitosan scaffolds for which the deacetylation process was carried out in 38 % NaOH solution.

2.3. Methods

2.3.1. Attenuated total reflectance Fourier transform infrared spectroscopy (ATR-FTIR)

The Fourier-transformed infrared spectra of all samples were recorded with a Nicolet iS50 FTIR spectrometer (Thermo Scientific, Inc., Waltham, MA, USA). The analyses were performed using a sophisticated built-in attenuated total reflectance (ATR) accessory, ensuring precise measurements. Measurements were made in a wavenumber range of 4000–400 cm^{-1}. The recorded spectra then underwent postprocessing, leveraging the advanced capabilities of OriginLab 2023 software (OriginPro, Version 2023, developed by OriginLab Corporation, Northampton, MA, USA). This detailed analysis and interpretation of the spectral data enabled insights into the structural characteristics and compositional variation within the samples.

2.3.2. Microscopy

Diverse microscopic techniques were employed for analysis. Digital microscopy involved the use of cutting-edge imaging systems, including the VHX-6000 digital microscope paired with VH-Z20R zoom lenses, providing magnifications up to 200 ×, alongside the Keyence VHX-7000 digital optical microscope equipped with VHX E20 zoom lenses (magnification up to 100 ×) and VHX E100 (magnification up to 500 ×), all supplied by Keyence (Osaka, Japan). Scanning electron microscopy was performed with the Quanta 250 FEG instrument (FEI Ltd., Czech Republic), complemented by an energy dispersive X-ray spectrometer with EDX Team Software for comprehensive analysis. The analyses also included fluorescence microscopy, using the Olympus IX73 Inverted Microscope operating within the spectral range Ex/Em = 460–495/510-IF nm, to elucidate specific fluorescence properties of the investigated samples.

2.3.3. Fluorescein isothiocyanate (FITC) staining

Fluorescein 5(6)-isothiocyanate (Sigma Aldrich, St. Louis, MO, USA) with a concentration of 2 mg/ml in ethanol was used for selective staining of chitosan. The chitin and chitosan samples were soaked in

prepared FITC solution and placed in the dark for 24 h. Afterwards, the samples were rinsed with distilled water with limited access to light until there was no change in the color of the rinsing water. Specimens were investigated using fluorescence microscopy.

2.3.4. Iodine test

Following the procedure outlined by Campbell (1929), a few drops of 5 % solution of iodine dissolved in potassium iodide were added to the samples, the excess solution was removed, and a few drops of a 1 % solution of sulfuric acid (STANLAB Sp. z o.o.) were added. The samples were thoroughly rinsed with distilled water. Specimens were investigated using digital light microscopy.

2.3.5. Cibacron Brilliant Red staining

Samples were soaked in a 0.3 % solution of Cibacron Brilliant Red 3B-A (Sigma Aldrich, St. Louis, MO, USA) and thoroughly washed with distilled water. Specimens were investigated using digital light microscopy.

2.3.6. Zeta potential tests

The surface zeta potential (SZP) of the 3D chitin/chitosan scaffold samples was calculated based on electro-osmotic measurements performed using a Zetasizer Nano ZS equipped with a surface zeta potential accessory (Malvern, UK). The tracers used were 1 ml of negatively charged carboxylated polystyrene latex particles (ZTS1240 Malvern, UK) and positively charged amidine polystyrene latex particles (Thermo Fisher Scientifics, USA) at the appropriate pH. The following conditions were applied for the measurements: 12.8° forward scatter with the attenuator in position 9, 2500–12000 kcps count rate, five distance position measurements at 125 μm steps, with five repetitions for each step (each measurement consisted of 30 sub-runs with a 60 s interval). The electro-osmotic tracer mobility was determined over 100 sub-runs. All measurements were made at 25 °C.

2.3.7. Synthesis of Cu nanocrystals

To determine the different complexing capacities of sponge chitin and chitin/ chitosan scaffold to copper(II) ions 10 mg of each material have been placed in 20 ml of 0.050 M $CuCl_2 \cdot 2\ NH_4\ Cl$ (Sigma-Aldrich) stock solution. Both scaffolds of pure chitin and chitin/chitosan origin remained in the copper solution for 24 h at room temperature. After that concentration of Cu^{2+} ions have been determined using OES.

The reduction of the copper(II) ions was carried out with fructose in a basic medium. 5 ml of a D-(-)-Fructose (Sigma-Aldrich) solution (150 mg/ml) was heated to approximately 60 °C in a Petri dish. After that four drops of 2.5 M NaOH have been added. After fructose begins to decompose (appearance of yellow colour), the chitin and chitin/chitosan scaffolds samples previously immersed within the stock solution under study and already complexed with copper have been given to the solution. Finally, the obtained samples were dialyzed against deionized water using 14 kDa membrane (Carl Roth, Germany). Dried on air specimens have been studied using SEM (ESEM XL 30, Phillips).

2.3.8. Optical emission spectroscopy (OES analysis)

The determination of the copper concentrations was carried out using the optical method Perkin-Elmer Optima 7000DV emission spectrometer.

2.3.9. Estimation of the degree of deacetylation

The evaluation method relies on forming ratios between the extreme values of the derivative spectrum for both measurement and reference bands. For this study, the FTIR derivative method uses the minimum at 1164 cm^{-1} as the reference point and the maximum at 1364 cm^{-1} as the measurement point. The 1164 cm^{-1} minimum is ideal as a reference because it represents the peak increase of the asymmetric C—O—C bridge stretching oscillation and is unaffected by the adjacent signal at 1204 cm^{-1}. This wavenumber range includes a stable plateau-like absorption due to water, minimizing its impact on sample measurements.

Spectra were normalized using the reference band at 1164 cm^{-1}. Only the extreme values of the amide III and symmetric CH_3 deformation oscillations are suitable for measurement. The amide I and amide II bands, however, are not ideal due to interference from atmospheric water vapor, which causes significant noise. The maximum at 1364 cm^{-1} was selected as the measurement band because it exhibits a consistent decline with increasing deacetylation.

ATR-FTIR calibration was conducted using chitin-chitosan samples obtained during deacetylation of *A. aerophoba* in a 38 % NaOH solution, along with chitin and chitosan standards. The acetylation levels were measured through UV/Vis analysis, as per Zivanovic's method (Wu & Zivanovic, 2008). The relationship between extreme value ratios and acetylation degrees follows a cubic polynomial. Interestingly, the curve's inflection point is near 50 % acetylation, indicating the transition between chitin and chitosan.

The acetylation levels of the chitin-chitosan composite samples under study were determined using the calibration function:

$$y = \left(2{\cdot}10^{-6}\right)^3 - \left(2,84{\cdot}10^{-4}\right)x^2 + \left(1,87{\cdot}10^{-2}\right)x + 0,154$$

The acetylation levels of the samples were calculated and presented in the Table 1.

2.3.10. Procedure of the reduction of 4-nitrophenol (4NP) to 4-aminophenol (4AP) (for details see Petrenko et al., 2019)

The 2.5 ml of aqueous solution of 4-nitrophenol (0.13 mM) was mixed with 0.5 ml freshly prepared aqueous solution of sodium borohydride (0.1 M) and yellow mixture was obtained. To the above solution an appropriate amount of catalyst was added to start reduction, the reaction was finished until the solution became colourless. During the reaction the mixture was continuously stirred and the progress of reaction was monitored using a UV-Vis spectrophotometer (Jasco V-750), the spectra was recorded after each 60 s of reaction.

The calculation of the reduction kinetics:

Due to the fact that concentration of $NaBH_4$ was much higher than concentration of 4-NP, it can be considered as constant during the reaction. Consequently, the reaction were concluded as pseudo-first order reaction model with respect to the concentration of 4-NP and reaction constant (k) was calculated from the Eq. (1):

$$\ln\left(\frac{C_t}{C_0}\right) = -kt \tag{1}$$

where, C_t is the concentration of 4-NP at the specified time t, C_0 is the initial concentration and k is the first-order rate constant (s^{-1}).

2.3.11. Nanoindentation

Nanomechanical measurements were performed with an Agilent G200 nanoindenter The instrument was calibrated before the measurement using the Oliver–Pharr method (Oliver& Pharr, 1992).

A DCMII measurement head was used, performing indentations with a maximum depth of 1600 nm. CSM mode was used during the

Table 1
Calculated acetylation degrees for the *A. aerophoba* chitin/chitosan samples obtained during deacetylation in 38 % NaOH solutions at 95 °C as well as *A. aerophoba* chitin, α-chitin and chitosan standards.

Sample	Acetylation degree
α-Chitin standard	86 %
A. aerophoba chitin	95 %
A. aerophoba chitin/chitosan 38 % 15 min	63 %
A. aerophoba chitin/chitosan 38 % 30 min	56 %
A. aerophoba chitin/chitosan 38 % 60 min	48 %
A. aerophoba chitin/chitosan 38 % 180 min	26 %
Chitosan standard	9 %

measurements. The indenter used was made of diamond and had a Berkovich-type geometry. Measurements were made on fibres immobilized in resin, at the centre of the fibre cross-section. Each fibre type was analysed by indentation at several locations for several fibres (n = 10) in a given series. Experimental data were statistically analysed through one-way ANOVA and Tukey's multiple pairwise comparisons test. A *p*-value of 0.05 was considered to be significantly different. Data are expressed as mean ± standard deviation (n = 10).

3. Results and discussion

3.1. Iodine test and Cibacron Brilliant Red staining

Identification of the chitosan layer on the surface of a chitin matrix is not a simple task. For this purpose, we took the methodological approaches described below. Careful staining analysis of chitin and chitosan was performed to visualize and to distinguish between these two structurally similar yet functionally distinct polysaccharides. Fig. 2 shows a series of digital microscopy images of *A. aerophoba* chitin and chitin/chitosan scaffold treated for 60 min in a 38 % NaOH solution, analyzed using both the iodine staining test and Cibacron Brilliant Red (CBR) dye.

The iodine test, also known as the van Weaseling method (Campbell, 1929), is useful for differentiating chitin from chitosan. Fig. 2 a and b depict the initial appearance of *A. aerophoba* chitin and chitin/chitosan scaffolds prior to staining. Upon treatment, chitosan displays a deep purple to nearly black hue, a color that remains stable even on thorough rinsing with deionized water (Fig. 2 d). Conversely, chitin initially

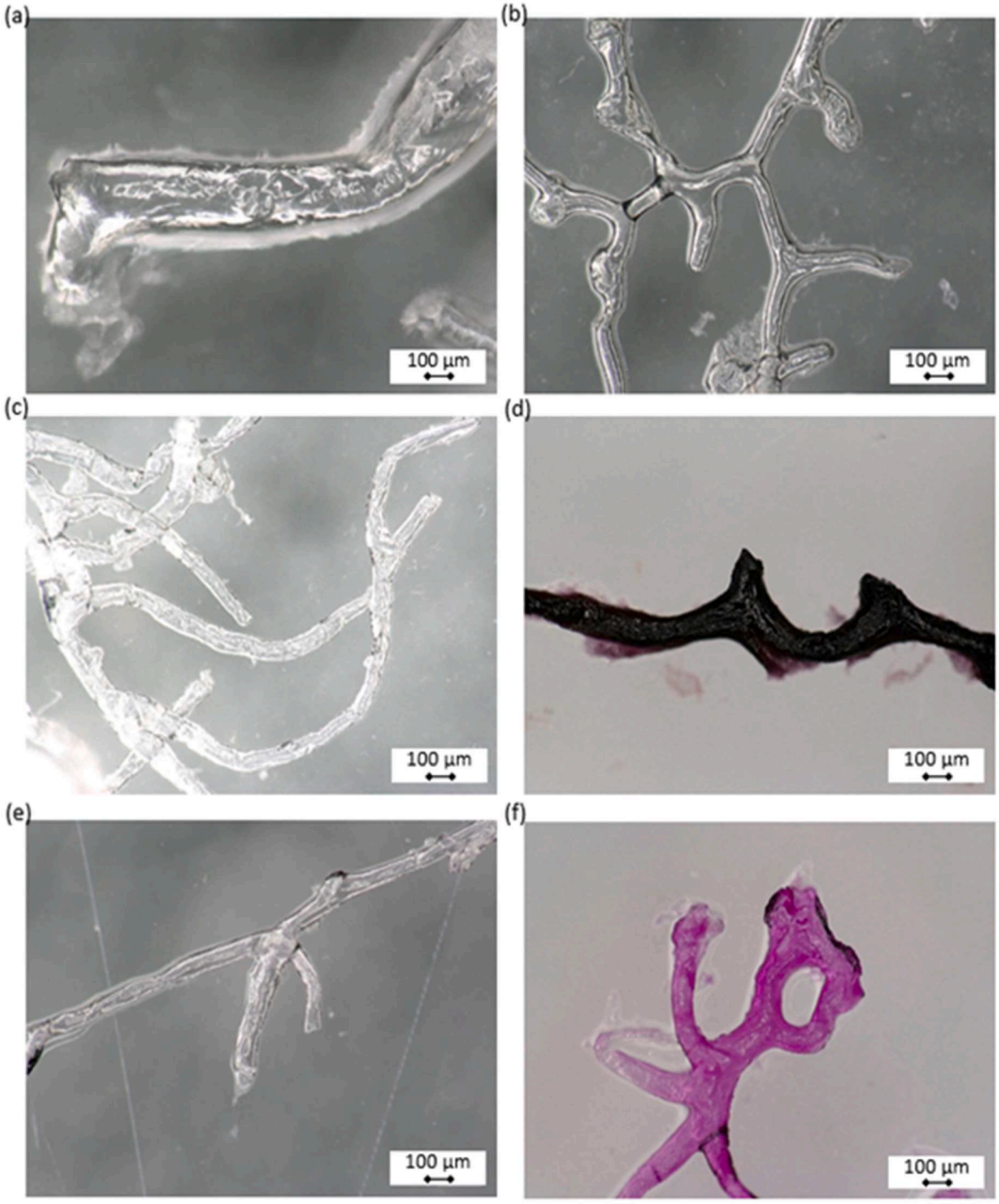

Fig. 2. Digital microscopy images showing *A. aerophoba* sponge chitin scaffold at various stages: (a) untreated, (c) post-iodine test, and (e) after CBR staining. No coloration is visible. In contrast, images of chitin/chitosan scaffold obtained after treatment with a 38 % NaOH solution for 60 min at 95 °C show (b) no color when untreated, (d) dark violet color after the iodine test, and (f) pink color after CBR staining. While chitin loses its color entirely upon washing with water, chitosan retains its coloration.

presents an orange or brown coloration that diminishes significantly with repeated washes, resulting in a substantially faded appearance (Fig. 2 c).

Cibacron Brilliant Red (CBR), widely recognized for its usefulness in quantifying chitosan concentrations via UV spectrophotometric methods (Hoffmann et al., 2016; Muzzarelli, 1998; Wischke & Borchert, 2006), produces a stark contrast in staining outcomes between chitosan and chitin. When applied to chitosan scaffolds, CBR imparts a vivid, durable pink coloration (Fig. 2 f). This color does not disappear upon washing with distilled water. In comparison, although chitin initially absorbs the CBR dye and appears pink, it loses this coloration rapidly upon rinsing, resulting in a discernibly paler hue (Fig. 2 e).

What are the specific binding interactions between iodine/Cibacron Brilliant Red dyes with the chitosan/chitin molecules? Chitosan, which contains free amino groups, easily binds with iodine. This interaction forms charge-transfer complexes that give a deep purple color. However, this color is unstable at room temperature and tends to fade over time (Yajima et al., 2001). In contrast, chitin typically produces only a faint brownish color that fades away after rinsing with water. This is due to chitin's acetylated structure, which does not interact with iodine (Kato et al., 1981).

Cibacron Brilliant Red dye forms much stronger and more specific bonds with chitosan through electrostatic interactions. The dye's sulfonic groups ($-SO_3^-$) bond to the protonated amino groups ($-NH_3^+$) in chitosan under acidic conditions, resulting in a bright, permanent stain (Hoffmann et al., 2016; Muedas-Taipe et al., 2020).

As stated by Giles and Hassan (1958), the hydroxyl groups in chitin are highly hydrated in water, which significantly limits their ability to form hydrogen bonds with dyes. Nevertheless, dyes can still adsorb onto chitin through the formation of hydrogen bonds, van der Waals interactions, and ion exchange with other chitin's functional groups (Giles & Hassan, 1958). This may explain the weaker and less stable chitin staining observed with Cibacron Brilliant Red.

These staining techniques not only facilitate visual differentiation between chitin and chitosan, but also underscore the distinct chemical and physical properties of these biopolymers. The persistent coloration of chitosan with both iodine and CBR dyes enables confirmation of its presence within the developed chitin/chitosan scaffolds.

3.2. *Attenuated total reflectance Fourier transform infrared spectroscopy (ATR-FTIR)*

Further analysis was carried out on the sample processed in a 38 % NaOH solution for 60 min, chosen for its good color retention during the iodine test compared with the corresponding sample processed for 15 min. FTIR analysis of this sample resulting from treatment of chitin for 60 min indicates a favorable chitin/chitosan balance, while the spectrum of the 30 min sample resembles that of chitin, and that of the 180 min sample is close to that of chitosan, implying that such treatment compromises the stability of the scaffold. Fig. 3 a, b shows the infrared spectra of all samples treated in 38 % NaOH solution, showing the gradual disappearance of the band around 1110 cm^{-1} in the 180 min sample, along with the shift of the chitin-characteristic band at 1428 cm^{-1} to 1417 cm^{-1} in both the 60- and 180 min samples, reflecting the behavior observed in the case of chitosan standards.

Additionally, for comparative purposes, Fig. 3 c, d present the FTIR spectrum for chitosan derived from *A. aerophoba* sponge after 60-minute treatment of sponge chitin in a 38 % NaOH solution at 95 °C. This is compared with the spectra of chitin and chitosan standards, alongside the spectrum of *A. aerophoba* sponge chitin. The chitosan product shows

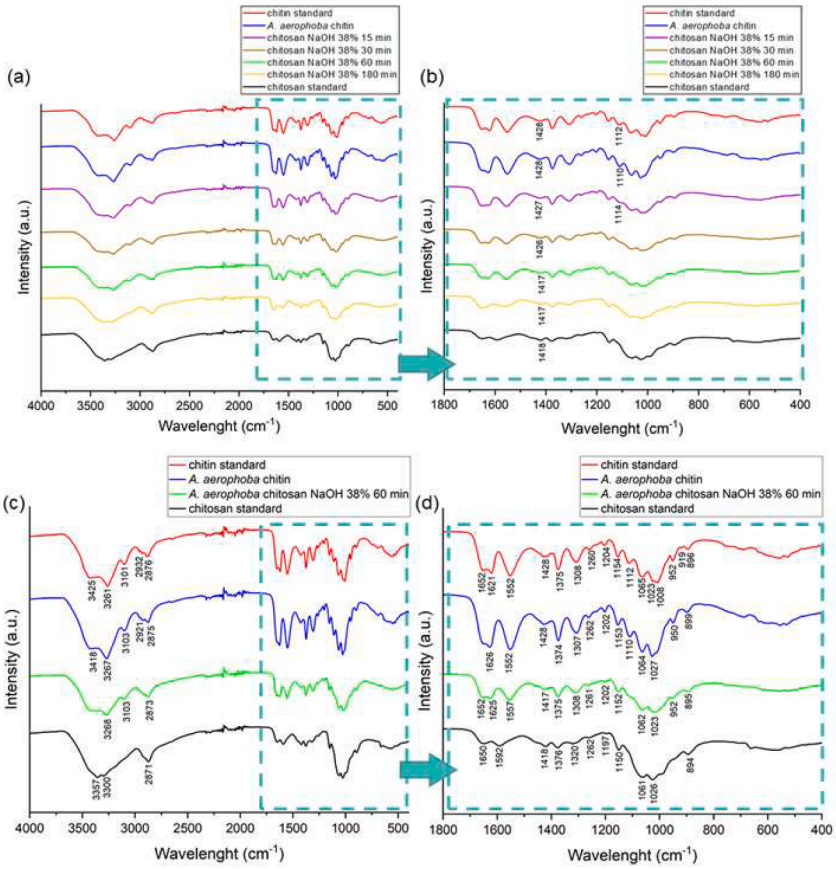

Fig. 3. ATR-FTIR spectra: of the samples obtained in 38 % NaOH solution, compared with chitin and chitosan standards as well as *A. aerophoba* sponge chitin, in the ranges (a, c) 4000–400 cm^{-1} and (b, d) 1800–400 cm^{-1}.

spectral characteristics akin to both the chitin and chitosan standards. Notably, its spectrum exhibits bands at 3103 cm^{-1} (indicative of N–H stretching vibrations), 1625 cm^{-1} (amide I vibrations), and 952 cm^{-1} (CH_3 wagging vibrations) that are similar to bands found in the chitin spectrum but not in the chitosan standard. Conversely, a band at 1417 cm^{-1}, which corresponds to CH_2 bending vibrations, matches the chitosan standard, deviating from the 1428 cm^{-1} band found in the chitin spectrum. Moreover, a band around 1110 cm^{-1}, associated with C–O–C and C–O stretching, is faintly present on the product's spectrum, in contrast to its pronounced appearance in the chitin spectrum and its absence in the spectrum of the chitosan standard. Details of the band wavelengths and their assignments are provided in Table 2. The optimal processing time for the newly developed 3D chitin/chitosan scaffolds was found to be 60 min, as that sample showed the desired balance between the properties of chitin and chitosan as indicated by FTIR analysis, while the 30 min sample was highly similar to chitin and the 180 min sample approached chitosan, threatening the stability of the scaffold.

3.3. Fluorescein isothiocyanate (FITC) staining

Fluorescein isothiocyanate (FITC) is commonly used to target and react with the amino groups present in chitosan, forming a fluorescent complex that facilitates the precise identification of chitosan within the samples (Lee et al., 2017; Li et al., 2015; Moussa et al., 2013; Zhao & Wu, 2006). Consequently, the differentiation of the chitin and chitin/chitosan samples under study was further advanced using fluorescent microscopy, a technique known for its high sensitivity and specificity. Fig. 4 presents fluorescent microscopy images of the samples after FITC staining. In the case of the pure *A. aerophoba* sponge chitin scaffold (Fig. 4 a) no characteristic fluorescence was observed, confirming the absence of the reactive amino groups typically associated with chitosan. Conversely, the obtained chitin/chitosan scaffold (Fig. 4 b) exhibited a distinct green fluorescence, indicative of successful FITC binding. Notably, the fluorescent intensity was higher along the outer walls of the fibers (indicated by a white arrow), while the centers of the fibers exhibited lower intensity (red arrow). This differential fluorescence pattern suggests a structural configuration in which the chitosan forms an outer layer around a core of chitin fiber (see also Fig. 5). Such an arrangement implies a partial deacetylation process, where the outer regions of the chitin fibers are more accessible to NaOH treatment, resulting in their conversion to chitosan. This observation is critical, as it underscores the heterogeneity within the treated samples, providing insights into the deacetylation dynamics and the resulting structural integrity of the biopolymer constructs.

Table 2
Wavenumbers from FTIR spectra of chitin and chitosan standards compared with *A. aerophoba* chitin and *A. aerophoba* chitosan obtained using 38 % NaOH solution for 60 min at 95 °C, and their assignments.

Chitin standard (cm^{-1})	*A. aerophoba* chitin (cm^{-1})	*A. aerophoba* chitosan (cm^{-1})	Chitosan standard (cm^{-1})	Peak assignment
3425	3418	-	3357	O-H stretching
3261	3267	3268	3300	N-H stretching
3101	3103	3103	-	N-H stretching
2932	2921	-	-	CH_x stretching
2876	2875	2873	2871	CH_x stretching
1652	-	1652	1650	Amide I
1621	1626	1625	-	Amide I
1552	1552	1557	1592	Amide II
1428	1428	1417	1418	CH_2 bending
1375	1374	1375	1376	CH_3 deformation
1308	1307	1308	1320	Amide III
1260	1262	1261	1262	Amide III
1204	1202	1202	1197	Amide III
1154	1153	1152	1150	C-O-C, C-O stretching
1112	1110	-	-	C-O-C, C-O stretching
1065	1064	1062	1061	C-O-C, C-O stretching
1023	1027	1023	1026	C-O-C, C-O stretching
1008	-	-	-	C-O stretch in phase ring
952	950	952	-	CH_3 wagging
896	899	895	894	CH ring stretching

The thickness of the chitosan layers was measured using ImageJ software (ImageJ 1.53t, National Institutes of Health, USA), revealing a range between 20 and 60 μm. The distribution of layer thickness was as follows: 29 % of the layers fell within the 20–30 μm range, 38 % within the 30–40 μm range, 24 % within the 40–50 μm range, and 10 % within the 50–60 μm range.

The optimal thickness range of chitosan layers for practical applications varies depending on the application and the desired mechanical, biochemical, or cell interaction properties.

For example, in skin regeneration and wound healing, the optimal thickness of chitosan layers ranges from 10 μm, where chitosan membranes in mesh form significantly promoted re-epithelialization and granular layer regeneration (Azad et al., 2004), to 60 ± 5 μm, where chitosan membranes with glycerol as a plasticizer demonstrated great wound healing properties (Ma et al. 2017), and up to less than 1 mm in the case of dermal regeneration (Haifei et al., 2014).

In the field of drug delivery, particularly for ocular applications, a thin chitosan-based film of around 3.5 μm was found to be optimal, offering high corneal permeability and rapid drug release (Li et al., 2020). The antibacterial activity and drug delivery properties can be adjusted by modifying pH and degree of deacetylation. The highest absorption of Rose Bengal dye (used as a model drug) occurred in the thickest hyaluronic acid and chitosan film, around 200 nm, as thicker films generally promote greater drug penetration and loading capacity (Rocha Neto et al., 2021).

For tissue engineering, chitosan membranes with a thickness of 60–80 μm were shown to support cell attachment and biodegradation, providing a favourable environment for fibroblast growth in skin tissue engineering (Ma et al., 2001). In corneal applications, films with a thickness of approximately 50 μm provided an optimal balance of mechanical stability, transparency, and permeability, making them ideal substrates for the attachment, proliferation, and implantation of autologous corneal endothelial cells, and highly suitable for minimally invasive procedures in corneal endothelial tissue engineering (Ozcelik et al., 2013). For cell proliferation studies, thicker chitosan membranes, particularly those between 90 and 170 μm, enhanced cell spreading, with mesenchymal stem cells and hepatocytes responding positively to increased membrane thickness (Uygun et al., 2010).

3.4. Microstructural observations

Initially, light microscopy was used to examine the surface morphology and structural characteristics of the obtained wet chitin/chitosan scaffolds. The appearance of a thin layer (Fig. 5) on the surface of this material that differs from the typical surface layers of poriferan chitin is well visible. To obtain more detailed information on structural changes of the surface of chitin scaffolds in comparison to that of the chitin/chitosan constructs, SEM studies were further carried out.

The SEM images presented in Fig. 6 offer a comparative visualization of *A. aerophoba* chitin fibers and their transformed product following deacetylation in a 38 % NaOH solution for 60 min at 95 °C. At lower magnifications (Fig. 6 a and c) the chitin fibers exhibit a typical smooth

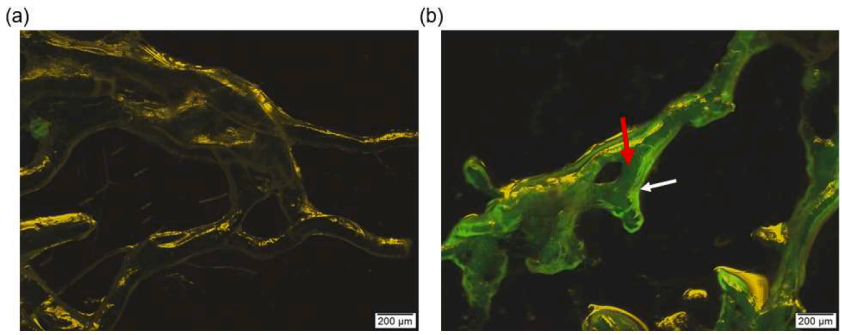

Fig. 4. Fluorescence microscopy images of (a) *A. aerophoba* sponge chitin scaffold and (b) the resulting chitin/chitosan scaffold after FITC staining. White arrow indicates intensive green fluorescence of chitosan layers on the scaffold; red arrow shows chitin core within the fiber. Light exposure time: (a) 109.7 ms, (b) 109.7 ms.

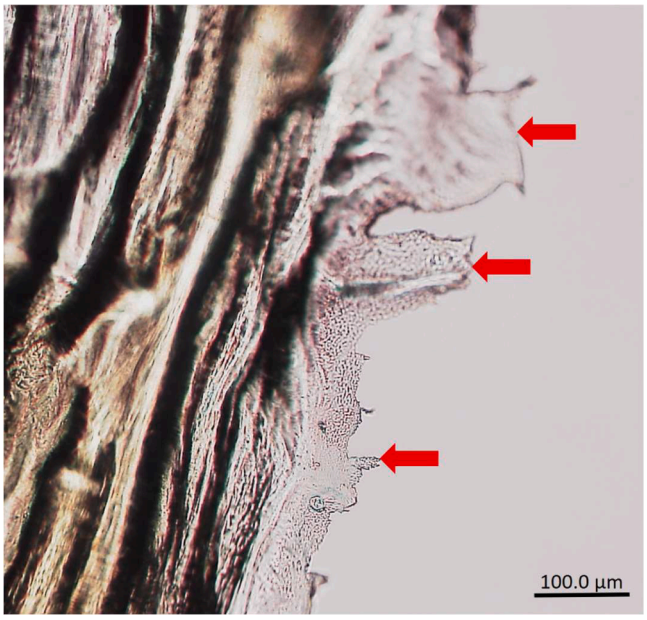

Fig. 5. Thin layer (arrows) on the surface of the studied chitin/chitosan scaffold, identified as chitosan, were well visible even under light microscopy observation.

and uniform appearance (see also Ehrlich et al., 2010), indicative of their natural, unmodified state. In contrast, the chitin/chitosan fibers (Fig. 6 b and d) display a noticeably ragged and irregular surface texture, highlighting the modification brought about by the deacetylation process. Upon closer examination at higher magnifications (Fig. 6 e and g) the chitin fibers reveal a characteristic wrinkled surface, a feature commonly noted in previous studies (Ehrlich et al., 2007, 2010). This wrinkling is likely due to the inherent structural properties of chitin, which remains intact in its native form. Conversely, the chitin/chitosan scaffold surfaces appear significantly smoother at higher magnifications (Fig. 6 f and h), suggesting a homogenization effect induced by the chemical modification process. This film-like smoothness can be attributed to the partial removal of acetyl groups during the deacetylation process, leading to a more uniform chitosan structure.

The sample of *A. aerophoba* sponge chitin/chitosan scaffold obtained from a 38 % NaOH solution after 60 min at 95 °C was further processed by dissolving it in a 1 % acetic acid solution. This step aimed to solubilize the chitosan component, leaving behind a residual scaffold that was subsequently rinsed with distilled water and subjected to freeze-drying. SEM images of the remaining scaffold, depicted in Fig. 7, reveal a fissured and rough surface, which is characteristic for chitin. These morphological features are significant, as they corroborate the hypothesis of a chitin core enveloped by a chitosan layer. The fissured appearance suggests that the outer chitosan layer was successfully dissolved in the acidic solution, revealing the underlying chitin structure. This dual-layer configuration, with a resilient chitin core and a versatile chitosan exterior, underscores the material's structural integrity and functional potential. The rough surface of the chitin scaffold observed in the SEM images (Fig. 7 a and b) aligns with the structural traits of native poriferan chitin, characterized by intrinsic rigidity and textural complexity.

The fissured nature of the surface further indicates the partial degradation or alteration of the chitin structure during the initial deacetylation process, which was not entirely smoothed out by the subsequent treatments. This observation of a chitin scaffold core with a chitosan layer is pivotal for applications requiring a combination of mechanical strength and chemical versatility. The robust chitin core provides structural support, while the chitosan layer offers a reactive surface for further chemical modifications or functionalization. Such a composite structure can be advantageous in various biomedical and industrial applications, including tissue engineering scaffolds, drug delivery systems, and bioactive coatings.

The changes in surface texture of chitin/chitosan fibers following deacetylation have significant implications for their applications, especially in biomedical fields like tissue engineering and drug delivery. For example, irregular and uneven surfaces created by deacetylation increase the biocompatibility of chitin/chitosan fibers. This texture promotes better cell adhesion and distribution, which is crucial for tissue engineering scaffolds. In the study by Rinaudo is discussed how chitosan's modified surface after deacetylation can facilitate improved interaction with fibroblasts, enhancing its suitability for skin tissue engineering applications (Rinaudo, 2006). However, for applications requiring smooth surfaces, such as in drug delivery systems, this texture may need to be controlled or minimized (Wilson et al., 2010) despite the rougher surfaces provide more binding sites for drug molecules, potentially improving the efficiency of drug delivery systems (Kumar, 2000). Except that, the introduction of an irregular surface texture via deacetylation affects the tensile strength and elasticity of chitosan (Ma et al., 2022), and these properties are crucial for applications requiring mechanical resilience, such as in load-bearing tissue scaffolds (Chander & Venkatraman, 2022; Correlo et al., 2010).

The textured surface of deacetylated chitin/chitosan fibers enhances their ability to adsorb contaminants from water, making them useful in environmental applications. The study by Crini et al. details how the increased surface area and available functional groups on chitosan beads improve their efficiency in removing heavy metals and dyes from wastewater (Crini, 2005).

The mechanical properties such as tensile strength and elasticity of chitosan can be enhanced through the introduction of an irregular surface texture via deacetylation. These properties are crucial for applications requiring mechanical resilience, such as in load-bearing tissue scaffolds.

(Chander & Venkatraman, 2022; Correlo et al., 2010). In the future

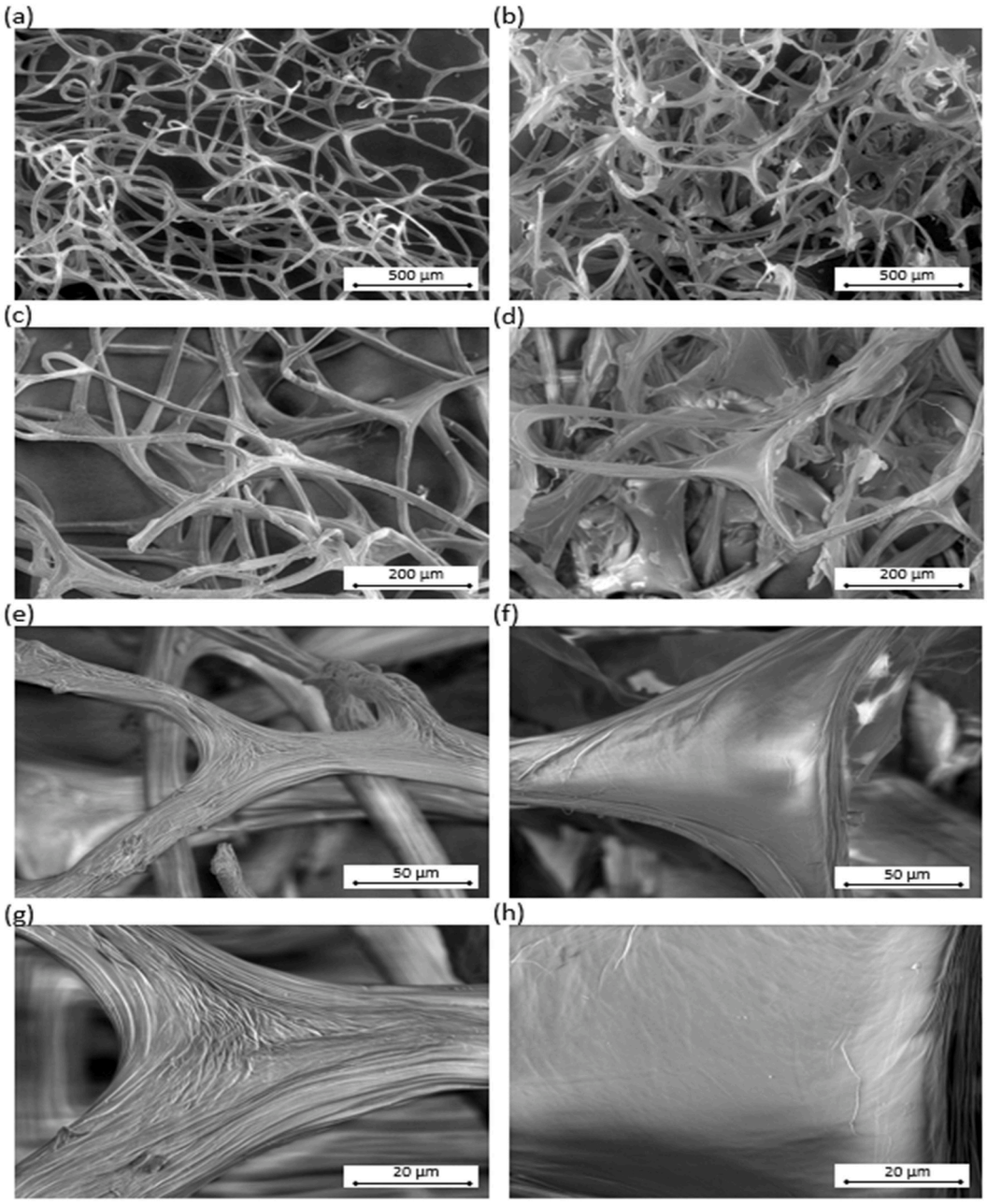

Fig. 6. SEM images of *A. aerophoba* chitin (a, c, e, g) and chitin/chitosan (b, d, f, h) resulting from treatment with a 38 % NaOH solution for 60 min at 95 °C, at different magnifications.

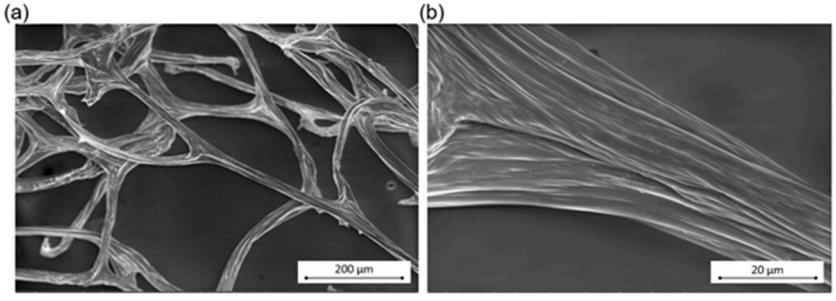

Fig. 7. SEM micrographs of *A. aerophoba* chitin/chitosan sample after dissolution in 1 % acetic acid reveal a chitin scaffold with a typical fissured surface.

studies we plan to investigate in details how do the differences in surface morphology of various chitin/chitosan scaffolds of sponges origin affect their mechanical properties. Surface morphology plays a critical role in determining the mechanical properties of chitin/chitosan scaffolds. Several studies have demonstrated how different aspects of scaffold morphology, such as porosity, fiber orientation, and surface modifications, influence their mechanical performance and biological compatibility.

According to several studies, such as those by Hutmacher (2000), increased porosity in chitin/chitosan scaffolds decreases mechanical strength but enhances biological properties like nutrient transport and cell migration. However, huge pores can weaken the overall mechanical stability.

A rougher surface can improve mechanical properties through better material bonding and enhanced interlocking with tissues or other materials. However, excessive roughness could act as a stress concentrator, weakening the scaffold over time. Aligned fibers within chitin/chitosan scaffolds can provide superior mechanical properties in the direction of alignment. Still, they may cause anisotropy in the structure, leading to lower mechanical performance in other directions (Nitti et al., 2018).

Surface modifications, such as coating chitosan scaffolds with selected bioactive molecules, also modulate biological and mechanical properties. For instance, chitosan-modified polycaprolactone scaffolds have been explored for their ability to sustain mechanical strength over time while supporting cell attachment and proliferation, making them promising for applications in ligament and tendon tissue engineering (Emonts et al., 2024; Silvestro et al., 2020).

3.5. Zeta potential tests

A. aerophoba chitin scaffolds before and after deacetylation of chitin were examined by the laser Doppler electrophoresis (LDE) technique. Although this method may be sensitive to surface homogeneity, the surface zeta potential of porous materials has been successfully determined. Since the goal of this study was to develop deacetylated chitosan scaffolds of sponge origin, the use of two latex tracer particles at pH 9.2 and pH 7 enabled a deep analysis of the raw and treated materials. A significant change in the material's charge after treatment dictated the use of positively and negatively charged tracer particles.

Fig. 8 a shows the measured SZP for chitin (orange bars) and chitosan (blue bars) samples, and the tracer zeta potential measured at a distance of 1000 μm from the surface in both buffers.

The SZP of chitin is close to the zeta potential value previously reported for chitin nanocrystals (Parajuli et al., 2022) at both pHs, with values of –1.39 mV ± 1.39 (R2= 0.965) for pH 9.2, and 7.95 mV ± 2.31 (R2= 0.971) for pH 7. Although the chitosan sample was not perfectly stable during the measurement, the surface zeta potential of –29.0 mV ± 5.17 (R2= 0.933) for pH 9.2 matches previously reported values (Alshahrani et al., 2021). The SZP values of –48.0 mV ± 18.7 (R2= 0.373) obtained for amidine tracer nanoparticles at pH 7 are questionable and could not be compared with the literature due to surface instability. This can be clearly seen in Fig. 8 b, where zeta potential vs. displacement is reported. The chitin sample was stable under both conditions, with no significant influence on the measurements. In contrast, chitosan samples tend to change their morphology (water

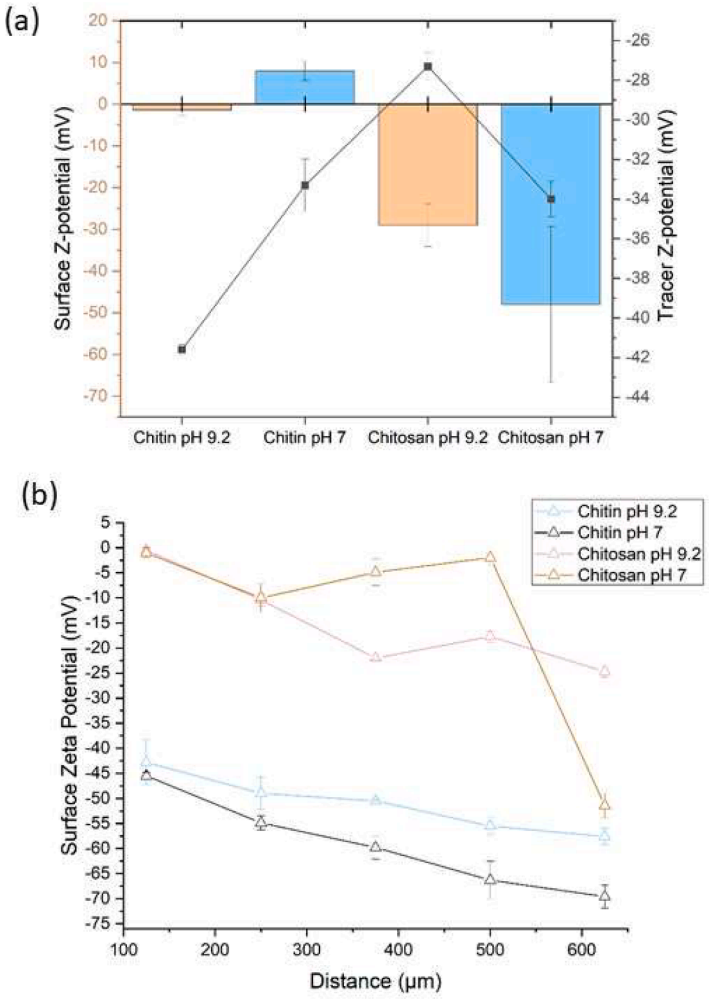

Fig. 8. Surface zeta potential (a) measured for chitin and chitosan; (b) as a function of displacement for the materials tested.

uptake, dispersion of micro-impurities, polymer diffusion from the material), as observed visually and during SZP measurement (measurement instability, significant measurement error). Although the chitosan sample is not stable at lower pH values, the laser Doppler technique was successfully used to monitor the sponge's surface zeta potential, confirming its successful modification.

As stated above, instability in chitosan samples was observed at lower pH levels. Several strategies can be employed to stabilize the surface of chitosan while retaining its functionality for applications such as catalysis or drug delivery to address its instability at lower pH levels. The instability typically arises because the amino groups on chitosan can protonate under acidic conditions, making the polymer soluble and less stable.

Cross-linking is one of the most common approaches to stabilizing chitosan. Chemical cross-linkers like glutaraldehyde, genipin, or ethylene glycol diglycidyl ether can form covalent bonds between chitosan chains, reducing solubility and enhancing mechanical and chemical stability. Cross-linked chitosan retains its functional groups' accessibility, allowing for continued interaction with substrates in catalysis or for controlled drug release. It is also less sensitive to pH changes, thus maintaining its structural integrity in acidic environments.

As alternative, ionic cross-linking can be also used. This procedure involves using multivalent anions, such as tripolyphosphate (TPP), to interact with the amine groups of chitosan. This non-covalent approach is reversible and can form stable hydrogels. Ionic cross-linking does not involve covalent bond formation, preserving the functional groups' reactivity. It provides stability against dissolution at lower pH by creating ionic bridges within the polymer matrix that are less susceptible to protonation (Agnihotri et al., 2004).

3.6. Metallization of 3D chitin/chitosan scaffold with copper

In principle, there are two suitable approaches for metallizing the chitin and chitin/chitosan scaffolds under study with respect to copper: the deposition of metal in the form of nanoparticles, or the reduction of metal ions directly on the surface of the scaffolds. It is well recognized that both chitin and chitosan show complexation properties with metal ions, especially transition elements, lanthanoids and actinides (Anastopoulos et al., 2017). However, chitosan if compared to chitin has a significantly higher potential for complex formation, i.e. it forms more stable complexes and can bind higher concentrations of metal ions (for overview see Gritsch et al., 2018; Matias et al., 2023). Chitosan shows particularly high affinities for copper ions (Rhazi et al., 2002; Usman et al., 2012). Chitosan has a higher potential for forming complexes with metal ions than chitin due to its unique chemical structure and functional groups (Kyzas & Bikiaris, 2015). The reason for this difference lies in the degree of deacetylation and the presence of free amino groups in chitosan that are unavailable in chitin. The primary functional groups in chitosan that facilitate the complexation with metal ions, particularly copper ions, are amino groups (-NH_2) (Rinaudo, 2006). These groups are located on the C-2 position of the glucosamine unit in chitosan. Amino groups are basic and can readily bind to metal ions through electron pair donation, forming coordinate covalent bonds. This interaction is typically more vital with transition metals like copper, which can accept electron pairs to complete their electron configuration.

Chitosan also contains hydroxyl groups at the C-3 and C-6 positions. While these groups can also interact with metal ions, their role is more supportive in stabilizing metal ion complexes through hydrogen bonding and other electrostatic interactions (Crini, 2005).

There are two different theories for the structure of the Cu-chitosan complex approaches. The first theory is called "bridge model" and describes four-fold coordination of the copper ion by nitrogen donor atoms of polymer chain or different chains. The "pendant model" describes the simple one coordination of the copper ion by an amine group (Matias et al., 2023). The formation of a five-membered ring chelate complex with the hydroxy group on the C_3 atom in the chitosan molecule has been suspected (Domard, 1987), but has not been proven experimentally.

In our study, the solution with placed chitin/chitosan scaffold showed intense blue colouring after 24 h. This will be on the formed copper(II)amine complex returned. Copper absorption on sponge chitin was measured as 4.5 μg/mg (2.8 %), however in the case of chitin/chitosan scaffold it reached a level of 77 μg/mg (48 %). It is striking that chitin complexes only very little amounts of copper. However, this matches with observations by Yaku and co-workers who found no copper complexation, for example, on chitin films (Rhazi et al., 2002).

It is well recognized that copper(II), for example, in copper sulfate solutions can be reduced with selected carbohydrates to obtain a copper powder (van der Weijden et al., 2002). In our study, the reduction of the copper(II) ions was carried out with fructose in a basic medium. In addition to possible enolization reactions, the degradation of the carbohydrate skeleton remains to be an essential characteristic of the base-catalyzed reaction. Fructose, as well as glucose and mannose are present via a common 1,2-enediol intermediate equilibrium. It occurs in the presence of oxidizing agents, e.g. Cu^{2+} for the oxidation of the enediol to form carboxylic acids. These are not stoichiometric. The alkaline reaction that occurs can also be used as qualitative evidence of reducing sugars known as Fehling's reaction. Due to the alkaline conditions, as well as the high temperature, chain breaks continue to occur due to retro-aldol reactions and caramelization. The intermediates formed can do more redox reactions, so that a complete reduction of the copper is possible. This phenomenon can be observed also in the case of our study using SEM. Microscopic images (Fig. 9) of the surface of sponge chitin and chitin/chitosan matrices after base catalysis reduction clearly show the deposition of nanocrystalline copper structures. The difference between two matrixes under study is well visible.

The obtained results opened the way for possible applications of 3D structured Cu-chitin/chitosan composites in corresponding catalysts as it has been reported previously for similar Cu-spongin composites of sponges' origin (Petrenko et al., 2019; Tsurkan et al., 2021).

Similarly to study on Cu/Cu_2O carbonized spongin scaffolds successfully used previously as catalyst in the reaction of reduction of 4-NP to 4-AP (Petrenko et al., 2019), we carried out preliminary experiments with developed here Cu-chitin/chitosan construct. In order to predict the mechanism of the catalitic abillity of Cu-chitin/chitosan material, the three-dimensional chitin isolated from *A. aerophoba* demosponge (Fig. 2 a), as well as piece of copper plate, were used as catalysts in the reduction of 4-NP under the same experimental conditions. It was observed that the 3D chitin scaffold does not possess catalytic ability towards 4-NP reduction. Interestingly, the copper plate is characterized by lower catalytic ability towards reduction of 4-nitrophenol, compared to Cu-chitin/chitosan based catalyst (rate constant 0.0043 s^{-1}). This results provide evidence that, the well-developed crystalline structure of Cu and Cu_2O onto created 3D scaffolds ensure sufficient active sites necessary for the rapid reduction of the 4-nitrophenol. It can be suggested that the Cu-chitin/chitosan based catalyst acts as a medium for transfer of electrons from BH^{4-} anions adsorbed at active sites of the catalyst to 4-NP particles, in order to produce 4-aminophenol. Similar results were reported by Sasmal and co-workers who studied the intriguing activity of the Cu_2O-Cu-CuO composite (Sasmal et al., 2016).

There are no doubts that metallization of chitin/chitosan scaffolds created in the study can significantly influence their mechanical properties, including tensile strength, elasticity, and durability. Metallization refers to the process of incorporating metal particles or ions into the scaffold matrix, often intended to enhance the scaffold's functional properties, such as conductivity or antimicrobial activity. Adding metal nanoparticles (like silver, gold, or copper) to chitosan scaffolds can enhance their tensile strength. This is due to the formation of stronger cross-links within the polymer matrix and between the polymer chains and metal ions. In some cases, excessive metallization or poorly dispersed metal particles can lead to agglomeration, which creates stress

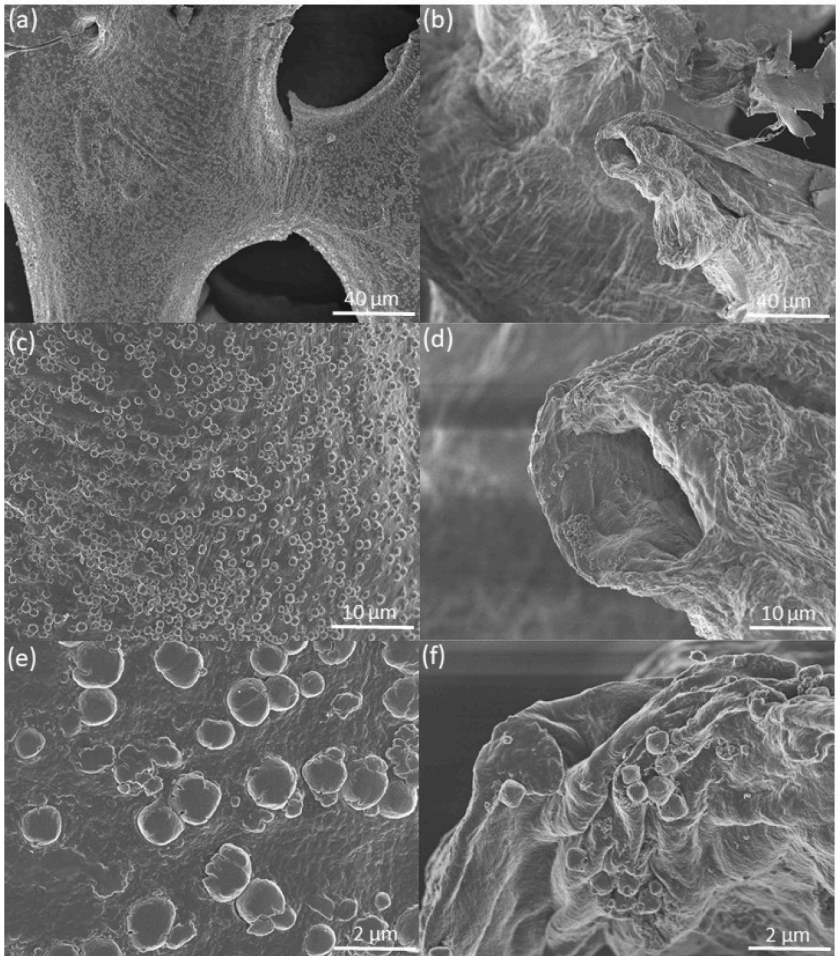

Fig. 9. SEM imagery of the surface of chitin/chitosan scaffold (a, c, e) in comparison to that of pure sponge chitin scaffold (b, d, f) after copper-based metallization using Cu^{2+} ion reduction in the presence of fructose under alkaline conditions.

concentration points within the scaffold and may reduce its tensile strength. Introducing rigid metal nanoparticles into the flexible polymeric matrix of chitosan can decrease the elasticity due to the stiffening effect of the metals, making the scaffold less deformable under stress. Metallization can enhance the durability of chitosan scaffolds, especially in terms of their resistance to microbial degradation and environmental stressors.

Fig. 10 shows the results of the elastic modulus (Fig. 10 a) and hardness (Fig. 10 b) tests (nanoindentation) for the 10 µm sections of *A. aerophoba* demosponge chitin, *A. aerophoba* Cu-chitin composite (Fig. 9 f) and *A. aerophoba* Cu-chitin/chitosan composite (Fig. 9 e). We suggest that the increase in the elastic modulus in the sample with Cu-chitin/chitosan composite is due to the presence of corresponding chitosan layers, and not to metallization with copper phase, which is present in the form of nanoparticles on the surface of the created material. There is no doubt that further detailed studies of the mechanical properties of the composite material we have obtained using various methods will provide new information that can become decisive in terms of the practical use of such novel 3D composites.

4. Conclusions

This study aimed, for the first time, to create chitosan layers on the surface of tubular sponge chitin fibers while preserving the three-dimensional architecture of the chitinous skeletal scaffold. This simple but innovative approach seeks to develop a unique chitin/chitosan composite matrix that retains the size and shape of the original chitin-based sponge skeleton, as exemplified by the cultivated *A. aerophoba* demosponge. The staining analysis employing iodine and Cibacron Brilliant Red (CBR) dyes enabled the clear differentiation of chitin from chitosan. Chitosan exhibits deep and durable coloration, whereas the color of chitin fades significantly upon washing. ATR-FTIR spectroscopy further elucidated the structural distinctions, indicating that a 60 min NaOH treatment yields an optimal chitin/chitosan balance. Fluorescent microscopy with FITC staining highlights the successful deacetylation process, as evidenced by the presence of amino groups in the chitosan. SEM analysis reveals notable morphological differences: chitin fibers maintain a smooth, uniform surface, while chitosan fibers exhibit a ragged texture, indicative of significant surface modifications. The identification of a dual-layer structure, with a chitosan exterior and chitin core, emphasizes the scaffold's mechanical strength and chemical versatility. Zeta potential measurements confirm the successful conversion of chitin to chitosan, despite observed instabilities at lower pH in chitosan samples. These findings highlight the potential of chitin/chitosan scaffolds in various biomedical and industrial applications, offering a scalable and adaptable manufacturing process that paves the way for future advancements in regenerative medicine and tissue engineering. Undoubtedly, the possible practical applications of the 3D chitin/chitosan scaffold created in this study will depend on extensive research to be carried out in the near future.

Funding

This work was supported by the National Science Center within the

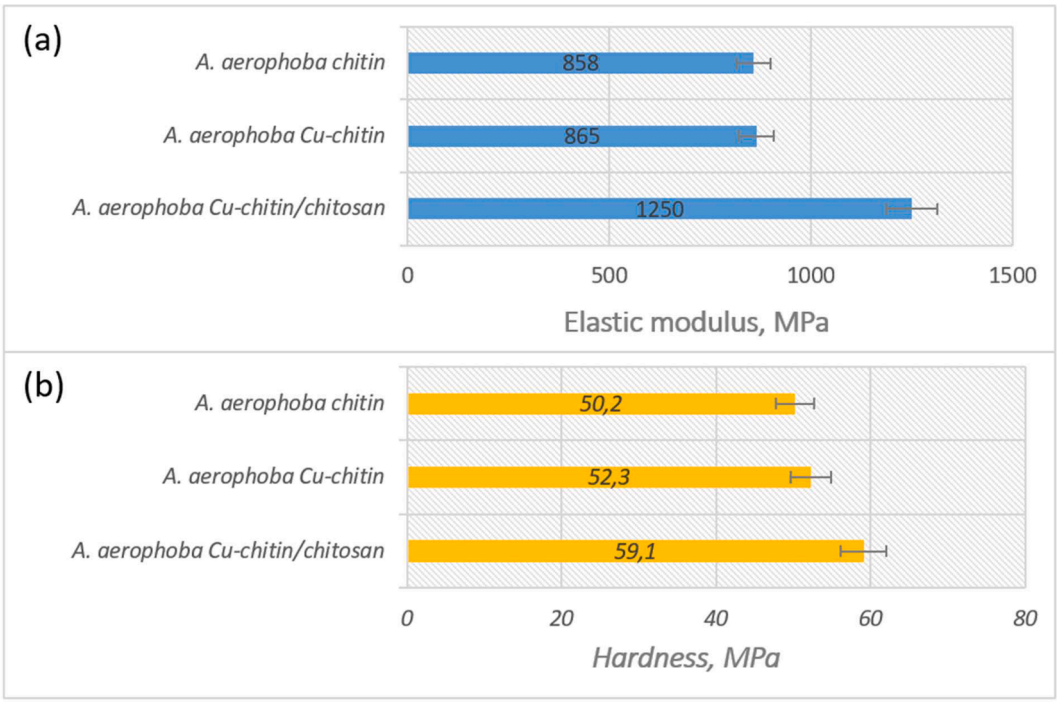

Fig. 10. Elastic modulus (a) and hardness (b) in megapascals (MPa) of 10 μm sections of *A. aerophoba* chitin, *A. aerophoba* Cu-chitin composite and *A. aerophoba* Cu-chitin/chitosan composite (± standard deviations).

framework of the OPUS 19 project, grant no. 2020/37/B/ST5/01909. Additionally, this work was supported by Ministry for Science and Higher Education as a subsidy to PUT (grant no. 0912/SBAD/2406)

CRediT authorship contribution statement

Izabela Dziedzic: Writing – original draft, Validation, Methodology, Investigation. **Kamil Dydek:** Writing – original draft, Methodology, Investigation, Data curation. **Jakub Trzciński:** Validation, Software, Methodology, Investigation. **Anna Boczkowska:** Visualization, Validation, Methodology, Data curation, Conceptualization. **Alona Voronkina:** Writing – original draft, Visualization, Methodology, Investigation, Data curation. **Teofil Jesionowski:** Writing – review & editing, Supervision, Resources, Project administration. **Hermann Ehrlich:** Writing – original draft, Project administration, Conceptualization.

Declaration of competing interest

The authors declare that they have no known competing financial interests or personal relationships that could have appeared to influence the work reported in this paper.

Data availability

Data will be made available on request.

References

Abdelaziz, A. G., Nageh, H., Abdo, S. M., Abdalla, M. S., Amer, A. A., Abdal-hay, A., & Barhoum, A. (2023). A review of 3D polymeric scaffolds for bone tissue engineering: principles, fabrication techniques, immunomodulatory roles, and challenges. *Bioengineering, 10*(2), 2. https://doi.org/10.3390/bioengineering10020204. Article.

Agnihotri, S. A., Mallikarjuna, N. N., & Aminabhavi, T. M. (2004). Recent advances on chitosan-based micro- and nanoparticles in drug delivery. *Journal of Controlled Release, 100*(1), 5–28.

Alshahrani, A. A., Alsuhybani, M., Algamdi, M. S., Alquppani, D., Mashhour, I., Alshammari, M. S., Alsohaimi, I. H., & Alraddadi, T. S. (2021). Evaluating the performance of chitosan and chitosan-palm membrane for water treatment: Preparation, characterization and purification study. *Journal of Taibah University for Science, 15*(1), 77–86. https://doi.org/10.1080/16583655.2021.1885192

Amato, A., Esposito, R., Federico, S., Pozzolini, M., Giovine, M., Bertolino, M., Guida, M., Manfra, L., Libralato, G., Zupo, V., & Costantini, M. (2024). Marine sponges as promising candidates for integrated aquaculture combining biomass increase and bioremediation: an updated review. Front. *Mar. Sci., 10*, Article 1234225. https://doi.org/10.3389/fmars.2023.1234225

Anandhavelu, S., Dhansekaran, V., Sethuraman, V., & Park, H. J. (2017). Chitin and chitosan based hybrid nanocomposites for super capacitor applications. *Journal of Nanoscience and Nanotechnology, 17*(2), 1321–1328. https://doi.org/10.1166/jnn.2017.12721

Anastopoulos, I., Bhatnagar, A., Bikiaris, D. N., & Kyzas, G. Z. (2017). Chitin adsorbents for toxic metals: A review. *International Journal of Molecular Sciences, 18*(1), 114. https://doi.org/10.3390/ijms18010114

Azad, A. K., Sermsintham, N., Chandrkrachang, S., & Stevens, W. F. (2004). Chitosan membrane as a wound-healing dressing: Characterization and clinical application. *Journal of Biomedical Materials Research Part B: Applied Biomaterials, 69B*(2), 216–222. https://doi.org/10.1002/jbm.b.30000

Beleño Acosta, B., Advincula, R. C., & Grande-Tovar, C. D. (2023). Chitosan-based scaffolds for the treatment of myocardial infarction: A systematic review. *Molecules (Basel, Switzerland), 28*(4), 1920. https://doi.org/10.3390/molecules28041920

Bergonzi, C., Di Natale, A., Zimetti, F., Marchi, C., Bianchera, A., Bernini, F., Silvestri, M., Bettini, R., & Elviri, L. (2019). Study of 3D-printed chitosan scaffold features after different post-printing gelation processes. *Scientific Reports, 9*(1), 362. https://doi.org/10.1038/s41598-018-36613-8

Bierwirth, J., Mantas, T. P., Villechanoux, J., & Cerrano, C. (2022). Restoration of marine sponges—what can we learn from over a century of experimental cultivation? *Water, 14*(7), 7. https://doi.org/10.3390/w14071055. Article.

Binnewerg, B., Schubert, M., Voronkina, A., Muzychka, L., Wysokowski, M., Petrenko, I., Djurović, M., Kovalchuk, V., Tsurkan, M., Martinovic, R., Bechmann, N., Fursov, A., Ivanenko, V. N., Tabachnick, K. R., Smolii, O. B., Joseph, Y., Giovine, M., Bornstein, S. R., Stelling, A. L., & Ehrlich, H. (2020). Marine biomaterials: Biomimetic and pharmacological potential of cultivated Aplysina aerophoba marine demosponge. *Materials Science and Engineering C, 109*, Article 110566. https://doi.org/10.1016/j.msec.2019.110566

Campbell, F. L. (1929). The detection and estimation of insect chitin; and the irrelation of "chitinization" to hardness and pigmentation of the Cuticula of the American cockroach, Periplaneta Americana L. *Annals of the Entomological Society of America, 22*(3), 401–426. https://doi.org/10.1093/aesa/22.3.401

Chander, N. G., & Venkatraman, J. (2022). Mechanical properties and surface roughness of chitosan reinforced heat polymerized denture base resin. *Journal of Prosthodontic Research, 66*(1), 101–108. https://doi.org/10.2186/jpr.JPR_D_20_00257

Choi, A. H., & Ben-Nissan, B. (2019). *Marine-Derived Biomaterials for Tissue Engineering Applications* (Eds.,, *14*. Springer. https://doi.org/10.1007/978-981-13-8855-2

Correlo, V. M., Costa-Pinto, A. R., Sol, P., Covas, J. A., Bhattacharya, M., Neves, N. M., & Reis, R. L. (2010). Melt processing of chitosan-based fibers and fiber-mesh scaffolds for the engineering of connective tissues. *Macromol Bioscience, 10*(12), 1495–1504. https://doi.org/10.1002/mabi.201000011

Crini, G. (2005). Recent developments in polysaccharide-based materials used as adsorbents in wastewater treatment. *Progress in Polymer Science, 30*(1), 38–70.

Duminis, T., Heljak, M., Święszkowski, W., Ereskovsky, A., Dziedzic, I., Nowicki, M., Pajewska-Szmyt, M., Voronkina, A., Bornstein, S. R., & Ehrlich, H. (2023). On the mechanical properties of microfibre-based 3D chitinous scaffolds from selected verongiida sponges. *Marine Drugs, 21*(9), 9. https://doi.org/10.3390/md21090463. Article.

Domard, A. (1987). pH and c.d. measurements on a fully deacetylated chitosan: Application to CuII-polymer interactions. *International Journal of Biological Macromolecules, 9*, 98–104. https://doi.org/10.1016/0141-8130(87)90033-X

Dziedzic, I., Voronkina, A., Pajewska-Szmyt, M., Kotula, M., Kubiak, A., Meissner, H., Duminis, T., & Ehrlich, H. (2023). The loss of structural integrity of 3D chitin scaffolds from aplysina aerophoba marine demosponge after treatment with LiOH. *Marine Drugs, 21*(6), 6. https://doi.org/10.3390/md21060334. Article.

Ehrlich, H., Ilan, M., Maldonado, M., Muricy, G., Bavestrello, G., Kljajic, Z., Carballo, J. L., Schiaparelli, S., Ereskovsky, A., Schupp, P., Born, R., Worch, H., Bazhenov, V. V., Kurek, D., Varlamov, V., Vyalikh, D., Kummer, K., Sivkov, V. V., Molodtsov, S. L., & Brunner, E. (2010). Three-dimensional chitin-based scaffolds from Verongida sponges (Demospongiae: Porifera). Part I. Isolation and identification of chitin. *International Journal of Biological Macromolecules, 47*(2), 132–140. https://doi.org/10.1016/j.ijbiomac.2010.05.007

Ehrlich, H., Luczak, M., Ziganshin, R., Mikšík, I., Wysokowski, M., Simon, P., Baranowska-Bosiacka, I., Kupnicka, P., Ereskovsky, A., Galli, R., Dyshlovoy, S., Fischer, J., Tabachnick, K. R., Petrenko, I., Jesionowski, T., Lubkowska, A., Figlerowicz, M., Ivanenko, V. N., & Summers, A. P. (2022). Arrested in Glass: Actin within sophisticated architectures of biosilica in sponges. *Advanced Science, 9*(11), Article 2105059. https://doi.org/10.1002/advs.202105059

Ehrlich, H., Maldonado, M., Spindler, K., Eckert, C., Hanke, T., Born, R., Goebel, C., Simon, P., Heinemann, S., & Worch, H. (2007). First evidence of chitin as a component of the skeletal fibers of marine sponges. Part I. Verongidae (demospongia: Porifera). *Journal of Experimental Zoology Part B: Molecular and Developmental Evolution, 308B*(4), 347–356. https://doi.org/10.1002/jez.b.21156

Ehrlich, H., Rigby, J. K., Botting, J. P., Tsurkan, M. V., Werner, C., Schwille, P., Petrášek, Z., Pisera, A., Simon, P., Sivkov, V. N., Vyalikh, D. V., Molodtsov, S. L., Kurek, D., Kammer, M., Hunoldt, S., Born, R., Stawski, D., Steinhof, A., Bazhenov, V. V., & Geisler, T. (2013). Discovery of 505-million-year old chitin in the basal demosponge Vauxia gracilenta. *Scientific Reports, 3*(1), 3497. https://doi.org/10.1038/srep03497

Ehrlich, H., Voronkina, A., Tabachnick, K., Kubiak, A., Ereskovsky, A., & Jesionowski, T. (2024). Silactins and structural diversity of biosilica in sponges. *Biomimetics, 9*(7), 7. https://doi.org/10.3390/biomimetics9070393. Article.

Ehrlich, H., Wysokowski, M., & Jesionowski, T. (2022). The philosophy of extreme biomimetics. *Sustainable Materials and Technologies, 32*, e00447. https://doi.org/10.1016/j.susmat.2022.e00447

Emonts, C., Bauer, B., Pitts, J., Roger, Y., Hoffmann, A., Menzel, H., & Gries, T. M (2024). Biological and in vitro degradation investigation of braided scaffolds for tendon and ligament tissue engineering based on different polycaprolactone materials with chitosan-graft-PCL surface modification. *Polymers, 16*, 2349. https://doi.org/10.3390/polym16162349

Flores-Jiménez, M. S., Garcia-Gonzalez, A., & Fuentes-Aguilar, R. Q. (2023). Review on porous scaffolds generation process: A tissue engineering approach. *ACS Applied Bio Materials, 6*(1), 1–23. https://doi.org/10.1021/acsabm.2c00740

Gholap, A. D., Rojekar, S., Kapare, H. S., Vishwakarma, N., Raikwar, S., Garkal, A., Mehta, T. A., Jadhav, H., Prajapati, M. K., & Annapure, U. (2024). Chitosan scaffolds: Expanding horizons in biomedical applications. *Carbohydrate Polymers, 323*, Article 121394. https://doi.org/10.1016/j.carbpol.2023.121394

Giles, C. H., & Hassan, A. S. A. (1958). Adsorption at organic surfaces V—A study of the adsorption of dyes and other organic solutes by cellulose and chitin. *Journal of the Society of Dyers and Colourists, 74*(12), 846–857. https://doi.org/10.1111/j.1478-4408.1958.tb02236.x

Gîjiu, C. L., Isopescu, R., Dinculescu, D., Memecică, M., Apetroaei, M.-R., Anton, M., Schröder, V., & Rău, I. (2022). Crabs marine waste—A valuable source of chitosan: tuning chitosan properties by chitin extraction optimization. *Polymers, 14*(21), 21. https://doi.org/10.3390/polym14214492. Article.

Gritsch, L., Lovell, C., Goldmann, W. H., & Boccaccini, A. R. (2018). Fabrication and characterization of copper(II)-chitosan complexes as antibiotic-free antibacterial biomaterial. *Carbohydr Polym, 1*(179), 370–378. https://doi.org/10.1016/j.carbpol.2017.09.095

Haifei, S., Xingang, W., Shoucheng, W., Zhengwei, M., Chuangang, Y., & Chunmao, H. (2014). The effect of collagen–chitosan porous scaffold thickness on dermal regeneration in a one-stage grafting procedure. *Journal of the Mechanical Behavior of Biomedical Materials, 29*(1), 114–125. https://doi.org/10.1016/j.jmbbm.2013.08.031

Harugade, A., Sherje, A. P., & Pethe, A. (2023). Chitosan: A review on properties, biological activities and recent progress in biomedical applications. *Reactive and Functional Polymers, 191*, Article 105634. https://doi.org/10.1016/j.reactfunctpolym.2023.105634

Hoffmann, S., Fuenzalida Werner, J. P., Moreno-Villoslada, I., & Goycoolea, F. M (2016). New insights into the nature of the Cibacron brilliant red 3B-A – Chitosan interaction. *Pure and Applied Chemistry, 88*(9), 891–904. https://doi.org/10.1515/pac-2016-0712

Hutmacher, D. W. (2000). Scaffolds in tissue engineering bone and cartilage. *Biomaterials, 21*(24), 2529–2543.

Jana, S., Florczyk, S. J., Leung, M., & Zhang, M. (2012). High-strength pristine porous chitosan scaffolds for tissue engineering. *Journal of Materials Chemistry, 22*(13), 6291–6299. https://doi.org/10.1039/C2JM16676C

Jesionowski, T., Norman, M., Żółtowska-Aksamitowska, S., Petrenko, I., Joseph, Y., & Ehrlich, H. (2018). Marine spongin: Naturally prefabricated 3D scaffold-based biomaterial. *Marine Drugs, 16*(3), 3. https://doi.org/10.3390/md16030088. Article.

Joseph, S. M., Krishnamoorthy, S., Paranthaman, R., Moses, J. A., & Anandharamakrishnan, C. (2021). A review on source-specific chemistry, functionality, and applications of chitin and chitosan. *Carbohydrate Polymer Technologies and Applications, 2*, Article 100036. https://doi.org/10.1016/j.carpta.2021.100036

Kadokawa, J. (2024). A mini-review: Fabrication of polysaccharide composite materials based on self-assembled chitin nanofibers. *Materials, 8*(8), 17. https://doi.org/10.3390/ma17081898. Article.

Kato, M., Mineshima, N., Kato, T., Kawada, Y., Hanada, T., Inomata, T. (1981). Chitosan-iodine adduct patent No. US4,275,194.

Kaya, M., Mujtaba, M., Ehrlich, H., Salaberria, A. M., Baran, T., Amemiya, C. T., Galli, R., Akyuz, L., Sargin, I., & Labidi, J. (2017). On chemistry of γ-chitin. *Carbohydrate Polymers, 176*, 177–186. https://doi.org/10.1016/j.carbpol.2017.08.076

Kaya, M., Ravikumar, P., Ilk, S., Mujtaba, M., Akyuz, L., Labidi, J., Salaberria, A. M., Cakmak, Y. S., & Erkul, S. K. (2018). Production and characterization of chitosan based edible films from *Berberis crataegina's* fruit extract and seed oil. *Innovative Food Science & Emerging Technologies, 45*, 287–297. https://doi.org/10.1016/j.ifset.2017.11.013

Kertmen, A., Dziedzic, I., & Ehrlich, H. (2023). Patentology of chitinous biomaterials. Part II: Chitosan. *Carbohydrate Polymers, 301*(Pt A), Article 120224. https://doi.org/10.1016/j.carbpol.2022.120224

Kertmen, A., & Ehrlich, H. (2022). Patentology of chitinous biomaterials. Part I: Chitin. *Carbohydrate Polymers, 282*, Article 119102. https://doi.org/10.1016/j.carbpol.2022.119102

Kertmen, A., Petrenko, I., Schimpf, C., Rafaja, D., Petrova, O., Sivkov, V., Nekipelov, S., Fursov, A., Stelling, A. L., Heimler, K., Rogoll, A., Vogt, C., & Ehrlich, H. (2021). Calcite nanotuned chitinous skeletons of giant ianthella basta marine demosponge. *International Journal of Molecular Sciences, 22*(22), 22. https://doi.org/10.3390/ijms222212588. Article.

Khrunyk, Y., Lach, S., Petrenko, I., & Ehrlich, H. (2020). Progress in modern marine biomaterials research. *Marine Drugs, 18*(12), 12. https://doi.org/10.3390/md18120589. Article.

Klinger, C., Żółtowska-Aksamitowska, S., Wysokowski, M., Tsurkan, M. V., Galli, R., Petrenko, I., Machałowski, T., Ereskovsky, A., Martinović, R., Muzychka, L., Smolii, O. B., Bechmann, N., Ivanenko, V., Schupp, P. J., Jesionowski, T., Giovine, M., Joseph, Y., Bornstein, S. R., Voronkina, A., & Ehrlich, H. (2019). Express method for isolation of ready-to-use 3D chitin scaffolds from Aplysina archeri (Aplysineidae: Verongiida) Demosponge. *Marine Drugs, 17*(2), 2. https://doi.org/10.3390/md17020131. Article.

Kou, S.(G), Peters, L. M., & Mucalo, M. R. (2021). Chitosan: A review of sources and preparation methods. *International Journal of Biological Macromolecules, 169*, 85–94. https://doi.org/10.1016/j.ijbiomac.2020.12.005

Kovalchuk, V., Voronkina, A., Binnewerg, B., Schubert, M., Muzychka, L., Wysokowski, M., Tsurkan, M. V., Bechmann, N., Petrenko, I., Fursov, A., Martinovic, R., Ivanenko, V. N., Fromont, J., Smolii, O. B., Joseph, Y., Giovine, M., Erpenbeck, D., Gelinsky, M., Springer, A., & Ehrlich, H. (2019). Naturally drug-loaded chitin: Isolation and applications. *Marine Drugs, 17*(10), 574. https://doi.org/10.3390/md17100574

Kozma, M., Acharya, B., & Bissessur, R. (2022). Chitin, chitosan, and nanochitin: extraction, synthesis, and applications. *Polymers, 14*(19), 19. https://doi.org/10.3390/polym14193989. Article.

Krishani, M., Shin, W. Y., Suhaimi, H., & Sambudi, N. S. (2023). Development of scaffolds from bio-based natural materials for tissue regeneration applications: A review. *Gels, 9*(2), 2. https://doi.org/10.3390/gels9020100. Article.

Królczyk, G.M., Wzorek, M., Król, A., Kochan, O., Su, J., & Kacprzyk, J. (Eds.). (2020). *Sustainable Production: Novel Trends in Energy, Environment and Material Systems* (Vol. 198). Springer International Publishing. https://doi.org/10.1007/978-3-030-11274-5.

Kumar, M. N. V. R. (2000). A review of chitin and chitosan applications. *Reactive and Functional Polymers, 46*(1), 1–27.

Kyzas, G. Z., & Bikiaris, D. N. (2015). Recent modifications of chitosan for adsorption applications: A critical and systematic review. *Marine Drugs, 13*(1), 312–337.

Lee, H., Kim, M., Yoon, Y., & Park, W. (2017). Fluorescent property of chitosan oligomer and its application as a metal ion sensor. *Marine Drugs, 15*(4), 105. https://doi.org/10.3390/md15040105

Li, B., Moriarty, T. F., Webster, T., & Xing, M. (2020). *Racing for the Surface: Antimicrobial and Interface Tissue Engineering* (Eds.). Springer International Publishing. https://doi.org/10.1007/978-3-030-34471-9

Li, B., Wang, J., Gui, Q., & Yang, H. (2020). Drug-loaded chitosan film prepared via facile solution casting and air-drying of plain water-based chitosan solution for ocular drug delivery. *Bioactive Materials, 5*(3), 577–583. https://doi.org/10.1016/j.bioactmat.2020.04.013

Li, H., Jiang, Z., Han, B., Niu, S., Dong, W., & Liu, W. (2015). Pharmacokinetics and biodegradation of chitosan in rats. *Journal of Ocean University of China, 14*(5), 897–904. https://doi.org/10.1007/s11802-015-2573-5

Lv, S. H. (2016). 7—High-performance superplasticizer based on chitosan. In F. Pacheco-Torgal, V. Ivanov, N. Karak, & H. Jonkers (Eds.), *Biopolymers and Biotech Admixtures for Eco-Efficient Construction Materials* (Eds., pp. 131–150). Woodhead Publishing. https://doi.org/10.1016/B978-0-08-100214-8.00007-5.

Ma, J., Wang, H., He, B., & Chen, J. (2001). A preliminary in vitro study on the fabrication and tissue engineering applications of a novel chitosan bilayer material as a scaffold of human neofetal dermal fibroblasts. *Biomaterials, 22*(4), 331–336. https://doi.org/10.1016/S0142-9612(00)00188-5

Ma, L., Su, W., Ran, Y., Ma, X., Yi, Z., Chen, G., Chen, X., Deng, Z., Tong, Q., Wang, X., & Li, X. (2020). Synthesis and characterization of injectable self-healing hydrogels based on oxidized alginate-hybrid-hydroxyapatite nanoparticles and carboxymethyl chitosan. *International Journal of Biological Macromolecules, 165*, 1164–1174. https://doi.org/10.1016/j.ijbiomac.2020.10.004

Ma, W., Zhang, S., Xie, C., Wan, X., Li, X., Chen, K., & Zhao, G. (2022). Preparation of high mechanical strength chitosan nanofiber/NanoSiO$_2$/PVA composite scaffolds for bone tissue engineering using Sol–Gel method. *Polymers, 14*, 2083. https://doi.org/10.3390/polym14102083

Ma, Y., Xin, L., Tan, H., Fan, M., Li, J., Jia, Y., Ling, Z., Chen, Y., & Hu, X. (2017). Chitosan membrane dressings toughened by glycerol to load antibacterial drugs for wound healing. *Materials Science and Engineering: C, 81*(12), 522–531. https://doi.org/10.1016/j.msec.2017.08.052

Matias, P. M. C., Sousa, J. F. M., Bernardino, E. F., Vareda, J. P., Durães, L., Abreu, P. E., Marques, J. M. C., Murtinho, D., & Valente, A. J. M. (2023). Reduced chitosan as a strategy for removing copper ions from water. *Molecules, 28*, 4110. https://doi.org/10.3390/molecules28104110

Moussa, S. H., Tayel, A. A., & Al-Turki, A. I. (2013). Evaluation of fungal chitosan as a biocontrol and antibacterial agent using fluorescence-labeling. *International Journal of Biological Macromolecules, 54*, 204–208. https://doi.org/10.1016/j.ijbiomac.2012.12.029

Muedas-Taipe, G., Mejía, I. M. M., Santillan, F. A., Velásquez, C. J., & Asencios, Y. J. O. (2020). Removal of azo dyes in aqueous solutions using magnetized and chemically modified chitosan beads. *Materials Chemistry and Physics, 256*(12), Article 123595. https://doi.org/10.1016/j.matchemphys.2020.123595

Mushi, N. E., Utsel, S., & Berglund, L. A. (2014). Nanostructured biocomposite films of high toughness based on native chitin nanofibers and chitosan. *Frontiers in Chemistry, 2*. https://doi.org/10.3389/fchem.2014.00099

Mutsenko, V., Gryshkov, O., Rogulska, O., Lode, A., Petrenko, A. Yu., Gelinsky, M., Glasmacher, B., & Ehrlich, H. (2019). Chitinous scaffolds from marine sponges for tissue engineering. In A. H. Choi, & B. Ben-Nissan (Eds.), *Marine-Derived Biomaterials for Tissue Engineering Applications* (Eds., pp. 285–307). Springer. https://doi.org/10.1007/978-981-13-8855-2_13.

Muzzarelli, R. A. A. (1998). Colorimetric determination of chitosan. *Analytical Biochemistry, 260*(2), 255–257. https://doi.org/10.1006/abio.1998.2705

Nikolova, M. P., & Chavali, M. S. (2019). Recent advances in biomaterials for 3D scaffolds: A review. *Bioactive Materials, 4*, 271–292. https://doi.org/10.1016/j.bioactmat.2019.10.005

Nitti, P., Gallo, N., Natta, L., Scalera, F., Palazzo, B., Sannino, A., & Gervaso, F. (2018). Influence of nanofiber orientation on morphological and mechanical properties of electrospun chitosan mats. *Journal of Healthc Engeneering, 13*, 3651480. https://doi.org/10.1155/2018/3651480

Nowacki, K., Galiński, M., Fursov, A., Voronkina, A., Meissner, H., Petrenko, I., Stelling, A. L., & Ehrlich, H. (2022). Electrolysis as a universal approach for isolation of diverse chitin scaffolds from selected marine demosponges. *Marine Drugs, 20*(11), 11. https://doi.org/10.3390/md20110665. Article.

Nuc, Z., & Dobrzycka-Krahel, A. (2021). From chitin to chitosan – A potential natural antimicrobial agent. *Progress on Chemistry and Application of Chitin and Its Derivatives, 26*, 23–40. https://doi.org/10.15259/PCACD.26.003

Oliver, W. C., & Pharr, G. M. (1992). An improved technique for determining hardness and elastic modulus using load and displacement sensing indentation experiments. *Journal of Material Research, 7*, 1564–1583.

Ozcelik, B., Brown, K. D., Blencowe, A., Daniell, M., Stevens, G. W., & Qiao, G. G. (2013). Ultrathin chitosan–poly(ethylene glycol) hydrogel films for corneal tissue engineering. *Acta Biomaterialia, 9*(5), 6594–6605. https://doi.org/10.1016/j.actbio.2013.01.020

Parajuli, S., Hasan, M. J., & Ureña-Benavides, E. E. (2022). Effect of the interactions between oppositely charged cellulose nanocrystals (CNCs) and chitin nanocrystals (ChNCs) on the enhanced stability of soybean oil-in-water emulsions. *Materials, 15*(19), 6673. https://doi.org/10.3390/ma15196673

Petrenko, I., Summers, A. P., Simon, P., Żółtowska-Aksamitowska, S., Motylenko, M., Schimpf, C., Rafaja, D., Roth, F., Kummer, K., Brendler, E., Pokrovsky, O. S., Galli, R., Wysokowski, M., Meissner, H., Niederschlag, E., Joseph, Y., Molodtsov, S., Ereskovsky, A., Sivkov, V., & Ehrlich, H. (2019). Extreme biomimetics: Preservation of molecular detail in centimeter-scale samples of biological meshes laid down by sponges. *Science Advances, 5*(10), eaax2805. https://doi.org/10.1126/sciadv.aax2805

Prem Ananth, K., & Jayram, N. D. (2024). A comprehensive review of 3D printing techniques for biomaterial-based scaffold fabrication in bone tissue engineering. *Annals of 3D Printed Medicine, 13*, Article 100141. https://doi.org/10.1016/j.stlm.2023.100141

Rhazi, M., Desbrieeres, J., Tolaimate, A., Rinaudo, M., Vottero, P., Alagui, A., & El Meray, M. (2002). Influence of the nature of the metal ions on the complexation with chitosan. Application to the treatment of liquid waste. *European Polymer Journal, 38*, 1523–1530.

Rinaudo, M. (2006). Chitin and chitosan: Properties and applications. *Progress in Polymer Science, 31*(7), 603–632.

Rocha Neto, J. B. M., Lima, G. G., Fiamingo, A., Germiniani, L. G. L., Taketa, T. B., Bataglioli, R. A., da Silveira, G. A. T., da Silva, J. V. L., Campana-Filho, S. P., Oliveira, O. N., Jr., & Beppu, M. M. (2021). Controlling antimicrobial activity and drug loading capacity of chitosan-based layer-by-layer films. *International Journal of Biological Macromolecules, 172*(3), 154–161. https://doi.org/10.1016/j.ijbiomac.2020.12.218

Sasmal, A. K., Dutta, S., & Pal, T. (2016). A ternary Cu$_2$O–Cu–CuO nanocomposite: a catalyst with intriguing activity. *Dalton Transactions, 45*(7), 3139–3150.

Schleuter, D., Günther, A., Paasch, S., Ehrlich, H., Kljajić, Z., Hanke, T., Bernhard, G., & Brunner, E. (2013). Chitin-based renewable materials from marine sponges for uranium adsorption. *Carbohydrate Polymers, 92*(1), 712–718. https://doi.org/10.1016/j.carbpol.2012.08.090

Schubert, M., Binnewerg, B., Voronkina, A., Muzychka, L., Wysokowski, M., Petrenko, I., Kovalchuk, V., Tsurkan, M., Martinovic, R., Bechmann, N., Ivanenko, V. N., Fursov, A., Smolii, O. B., Fromont, J., Joseph, Y., Bornstein, S. R., Giovine, M., Erpenbeck, D., Guan, K., & Ehrlich, H. (2019). Naturally prefabricated marine biomaterials: isolation and applications of flat chitinous 3D scaffolds from ianthella labyrinthus (Demospongiae: Verongiida). *International Journal of Molecular Sciences, 20*(20), 20. https://doi.org/10.3390/ijms20205105. Article.

Shimojo, A. A. M., Rodrigues, I. C. P., Perez, A. G. M., Souto, E. M. B., Gabriel, L. P., & Webster, T. (2020). Scaffolds for tissue engineering: a state-of-the-art review concerning types, properties, materials, processing, and characterization. In B. Li, T. F. Moriarty, T. Webster, & M. Xing (Eds.), *Racing for the Surface: Antimicrobial and Interface Tissue Engineering* (Eds., pp. 647–676). Springer International Publishing. https://doi.org/10.1007/978-3-030-34471-9_23.

Silvestro, I., Francolini, I., Di Lisio, V., Martinelli, A., Pietrelli, L., Scotto d'Abusco, A., Scoppio, A., & Piozzi, A. (2020). Preparation and characterization of TPP-chitosan crosslinked scaffolds for tissue engineering. *Materials, 13*, 3577. https://doi.org/10.3390/ma13163577

Sivanesan, I., Muthu, M., Gopal, J., Hasan, N., Kashif Ali, S., Shin, J., & Oh, J.-W. (2021). Nanochitosan: Commemorating the metamorphosis of an ExoSkeletal waste to a versatile nutraceutical. *Nanomaterials, 11*(3), 3. https://doi.org/10.3390/nano11030821. Article.

Sivashankari, P. R., & Prabaharan, M. (2017). 5—Deacetylation modification techniques of chitin and chitosan. In J. A. Jennings, & J. D. Bumgardner (Eds.), *Chitosan Based Biomaterials Volume 1* (Eds., pp. 117–133). Woodhead Publishing. https://doi.org/10.1016/B978-0-08-100230-8.00005-4.

Sogias, I. A., Williams, A. C., & Khutoryanskiy, V. V. (2008). Why is chitosan mucoadhesive? *Biomacromolecules, 9*(7), 1837–1842. https://doi.org/10.1021/bm800276d

Suamte, L., Tirkey, A., Barman, J., & Jayasekhar Babu, P. (2023). Various manufacturing methods and ideal properties of scaffolds for tissue engineering applications. *Smart Materials in Manufacturing, 1*, Article 100011. https://doi.org/10.1016/j.smmf.2022.100011

Talevski, T., Talevska Leshoska, A., Pejoski, E., Pejin, B., Machałowski, T., Wysokowski, M., Tsurkan, M. V., Petrova, O., Sivkov, V., Martinovic, R., Pantovic, S., Khrunyk, Y., Trylis, V., Fursov, A., Djurovic, M., Jesionowski, T., & Ehrlich, H. (2020). Identification and first insights into the structure of chitin from the endemic freshwater demosponge *Ochridaspongia rotunda* (Arndt, 1937). *International Journal of Biological Macromolecules, 162*, 1187–1194. https://doi.org/10.1016/j.ijbiomac.2020.06.247

Tsurkan, D., Simon, P., Schimpf, C., Motylenko, M., Rafaja, D., Roth, F., Inosov, D. S., Makarova, A. A., Stepniak, I., Petrenko, I., Springer, A., Langer, E., Kulbakov, A. A., Avdeev, M., Stefankiewicz, A. R., Heimler, K., Kononchuk, O., Hippmann, S., Kaiser, D., & Ehrlich, H. (2021). Extreme biomimetics: Designing of the first nanostructured 3D spongin–atacamite composite and its application. *Advanced Materials, 33*(30), Article 2101682. https://doi.org/10.1002/adma.202101682

Tsurkan, M. V., Voronkina, A., Khrunyk, Y., Wysokowski, M., Petrenko, I., & Ehrlich, H. (2021). Progress in chitin analytics. *Carbohydrate Polymers, 252*, Article 117204. https://doi.org/10.1016/j.carbpol.2020.117204

Tyliszczak, B., Drabczyk, A., Kudłacik-Kramarczyk, S., & Sobczak-Kupiec, A. (2020). Sustainable production of chitosan. In G. M. Królczyk, M. Wzorek, A. Król, O. Kochan, J. Su, & J. Kacprzyk (Eds.), *Sustainable Production: Novel Trends in Energy, Environment and Material Systems* (Eds., pp. 45–60). Springer International Publishing. https://doi.org/10.1007/978-3-030-11274-5_4.

Unnithan, A. R., Sasikala, A. R. K., Thomas, S. S., Nejad, A. G., Cha, Y. S., Park, C. H., & Kim, C. S. (2018). Strategic design and fabrication of biomimetic 3D scaffolds: unique architectures of extracellular matrices for enhanced adipogenesis and soft tissue reconstruction. *Scientific Reports, 8*(1), 5696. https://doi.org/10.1038/s41598-018-23966-3

Usman, M. S., Ibrahim, N. A., Shameli, K., Zainuddin, N., & Yunus, W. M. (2012). Copper nanoparticles mediated by chitosan: Synthesis and characterization via chemical methods. *Molecules, 17*(12), 14928–14936. https://doi.org/10.3390/molecules171214928

Uygun, B. E., Bou-Akl, T., Albanna, M., & Matthew, H. W. T. (2010). Membrane thickness is an important variable in membrane scaffolds: Influence of chitosan membrane structure on the behavior of cells. *Acta Biomaterialia, 6*(6), 2126–2131. https://doi.org/10.1016/j.actbio.2009.11.018

van der Weijden, D., Mahabir, J., Abbadi, A., & Reuter, M. A. (2002). Copper recovery from copper(II) sulfate solutions by reduction with carbohydrates. *Hydrometallurgy, 64*, 131–146.

Voronkina, A., Romanczuk-Ruszuk, E., Przekop, R. E., Lipowicz, P., Gabriel, E., Heimler, K., Rogoll, A., Vogt, C., Frydrych, M., Wienclaw, P., Stelling, A. L., Tabachnick, K., Tsurkan, D., & Ehrlich, H. (2023). Honeycomb biosilica in sponges: From understanding principles of unique hierarchical organization to assessing biomimetic potential. *Biomimetics, 8*(2), 2. https://doi.org/10.3390/biomimetics8020234. Article.

Wilson, B., Samanta, M. K., Santhi, K., Kumar, K. P., Ramasamy, M., & Suresh, B. (2010). Chitosan nanoparticles as a new delivery system for the anti-Alzheimer drug tacrine. *Nanomedicine, 6*(1), 144–152. https://doi.org/10.1016/j.nano.2009.04.001

Wischke, C., & Borchert, H.-H. (2006). Increased sensitivity of chitosan determination by a dye binding method. *Carbohydrate Research, 341*(18), 2978–2979. https://doi.org/10.1016/j.carres.2006.10.012

Wu, T., & Zivanovic, S. (2008). Determination of the degree of acetylation (DA) of chitin and chitosan by an improved first derivative UV method. *Carbohydrate Polymers, 2* (73), 248–253. https://doi.org/10.1016/j.carbpol.2007.11.024

Wysokowski, M., Machałowski, T., Idaszek, J., Chlanda, A., Jaroszewicz, J., Heljak, M., Niemczak, M., Piasecki, A., Gajewska, M., Ehrlich, H., Święszkowski, W., & Jesionowski, T. (2023). Deep eutectic solvent-assisted fabrication of bioinspired 3D carbon–calcium phosphate scaffolds for bone tissue engineering. *RSC Advances, 13* (32), 21971–21981. https://doi.org/10.1039/D3RA02356G

Wysokowski, M., Petrenko, I., Stelling, A. L., Stawski, D., Jesionowski, T., & Ehrlich, H. (2015). Poriferan chitin as a versatile template for extreme biomimetics. *Polymers, 7* (2), 2. https://doi.org/10.3390/polym7020235. Article.

Xing, L., Fan, Y.-T., Zhou, T.-J., Gong, J.-H., Cui, L.-H., Cho, K.-H., Choi, Y.-J., Jiang, H.-L., & Cho, C.-S. (2018). Chemical modification of chitosan for efficient vaccine delivery. *Molecules, 23*(2), 2. https://doi.org/10.3390/molecules23020229. Article.

Yajima, H., Morita, M., Hashimoto, M., Sashiwa, H., Kikuchi, T., & Ishii, T. (2001). Complex formation of chitosan with iodine and its structure and spectroscopic properties—Molecular assembly and thermal hysteresis behavior. *International Journal of Thermophysics, 22*, 1265–1283. https://doi.org/10.1023/A:1010628712529

Younes, I., & Rinaudo, M. (2015). Chitin and chitosan preparation from marine sources. structure, properties and applications. *Marine Drugs, 13*(3), 3. https://doi.org/10.3390/md13031133. Article.

Zhao, J., & Wu, J. (2006). Preparation and characterization of the fluorescent chitosan nanoparticle probe. *Chinese Journal of Analytical Chemistry, 34*(11), 1555–1559. https://doi.org/10.1016/S1872-2040(07)60015-2